UNCLASSIFIED

SECURITY CLASSIFICATION OF THIS PAGE

(2)

ORT DOCUMENTATION PAGE

AD-A216 687

1b. RESTRICTIVE MARKINGS	
2a	3. DISTRIBUTION/AVAILABILITY OF REPORT: ~~Restricted~~ unlimited
2b. DECLASSIFICATION/DOWNGRADING SCHEDULE	
4. PERFORMING ORGANIZATION REPORT NUMBER(S)	5. MONITORING ORGANIZATION REPORT NUMBER(S): AFOSR-TR-89-1758
6a. NAME OF PERFORMING ORGANIZATION: Dept of Materials Science & Engineering M.I.T.	6b. OFFICE SYMBOL (If applicable):
7a. NAME OF MONITORING ORGANIZATION: AFOSR/NC	
6c. ADDRESS (City, State and ZIP Code): 77 Massachusetts Avenue, Cambridge, MA 02139	7b. ADDRESS (City, State and ZIP Code): Bldg 410, Bolling AFB, DC 20332-6448
8a. NAME OF FUNDING/SPONSORING ORGANIZATION: AFOSR	8b. OFFICE SYMBOL (If applicable): NC
9. PROCUREMENT INSTRUMENT IDENTIFICATION NUMBER: AFOSR-81-0011	
8c. ADDRESS (City, State and ZIP Code): Bldg 410, Bolling AFB, DC 20332-6448	10. SOURCE OF FUNDING NOS.

PROGRAM ELEMENT NO.	PROJECT NO.	TASK NO.	WORK UNIT NO.
61102F			

11. TITLE (Include Security Classification): Ceramics Derived From Organo-Metallic Precursors & Microstructure of Amorphous Polymer

12. PERSONAL AUTHOR(S)

TYPE OF REPORT	13b. TIME COVERED	14. DATE OF REPORT (Yr., Mo., Day)	15. PAGE COUNT
Final	FROM ____ TO ____	Jul 1985	

16. SUPPLEMENTARY NOTATION

17. COSATI CODES			18. SUBJECT TERMS (Continue on reverse if necessary and identify by block number)
FIELD	GROUP	SUB. GR.	

19. ABSTRACT (Continue on reverse if necessary and identify by block number)

20. DISTRIBUTION/AVAILABILITY OF ABSTRACT

ASSIFIED/UNLIMITED ☐ SAME AS RPT. ☐ DTIC USERS ☐

21. ABSTRACT SECURITY CLASSIFICATION: UNCLASSIFIED

22a. NAME OF RESPONSIBLE INDIVIDUAL	22b. TELEPHONE NUMBER (Include Area Code)	22c. OFFICE SYMBOL
Dr. Donald R. Ulrich	202-767-4963	NC

DD FORM 1473, 83 APR EDITION OF 1 JAN 73 IS OBSOLETE.

UNCLASSIFIED

SECURITY CLASSIFICATION OF THIS PAGE

FINAL REPORT

CERAMICS DERIVED FROM ORGANO-METALLIC PRECURSORS AND MICROSTRUCTURE OF AMORPHOUS POLYMER

AFOSR-81-0011

Massachusetts Institute of Technology

77 Massachusetts Avenue

Cambridge, MA 02139

Professor Donald R. Uhlmann

July 1985

I. INTRODUCTION

During the past year, the research carried out under the grant was directed to two areas: (1) the development of microstructure in thermosetting resins, most notably epoxy resins; and (2) the exploration of the chemistry and kinetic processes involved in the conversion of organometallic materials to ceramics. Progress in each of these areas will be summarized in the sections which follow.

The student working on the development of microstructure in thermosetting resins will complete his doctoral thesis in September. His place will be taken by a second graduate student investigating the conversion of organo-metallic precursors to ceramics. As indicated in the appended proposal, the latter area will represent the exclusive focus of our work for the coming year.

II. MICROSTRUCTURE OF EPOXY RESINS

The present work represented a continuation of our efforts directed to understanding the microstructure of epoxy resin cured with amine hardeners. The focus has been on characterizing a series of networks formed by changing the formulations and the processing conditions of the system. The morphological analysis has been supplemented by a statistical model for the network formation; and the results have been used to understand and control the mechanical properties of these materials.

The table on ~~the following~~ page 3 shows the Epon 828 epoxy/triethylene tetramine (TETA) formulations which were explored, together with the curing conditions employed.

Figure 1 shows the glass transition temperatures (T_g) of these specimens. Table 2 shows the molecular weight between the crosslinks (M_c) for some of the formulations. M_c was evaluated from the rubbery modulus of the resins after applying rubber elasticity theory. The epoxy-rich formulations have higher M_c, which decreases towards the stoichiometric formulations, and then again increases with increasing curing agent concentration. M_c decreased after the post curing treatment. A relationship has been found between T_g and M_c:

$$T_g = 51.7 + 23800/M_c \qquad (1)$$

The modulus at room temperature of these resins is shown in Figure 2. The modulus decreases with increasing hardener content, especially around stoichiometry. From the published literature, epoxies have been assigned a two phase structure (nodular) from an analysis of their fracture surfaces and dynamic mechanical properties. The dispersed phase accounts for more

TABLE 1

EPON/TETA Formulations

Condition	Concentration of Curing Agent, PHR	Epoxide/Amine Hydrogen (E/A)	Curing Condition* hour , C
A	6.5	2:1	7,120
B	6.5	2:1	4 RT/7,120
C	8	1.63:1	4 RT/7,120
E	10	1.3:1	7,120
F	10	1.3:1	4 RT/3,83
G	10	1.3:1	4 RT/8,83
H	12	1.06:1	1 RT/8,83
I1	13	1:1	7,110
I2	13	1:1	7,110
K1	13	1:1	8,83
K2	13	1:1	8,83
L1	13	1:1	1 RT/8,83
L2	13	1:1	1 RT/8,83
M	17	1:1.3	12,80
N	17	1:1.3	3 RT/9,80
Q	26	1:2	12,80
R	26	1:2	3 RT/9,80

*RT is Room Temperature.

A part of each of the samples was also subjected to Postcure at 150 C for two hours. This will be indicated in the text by a superscript P.

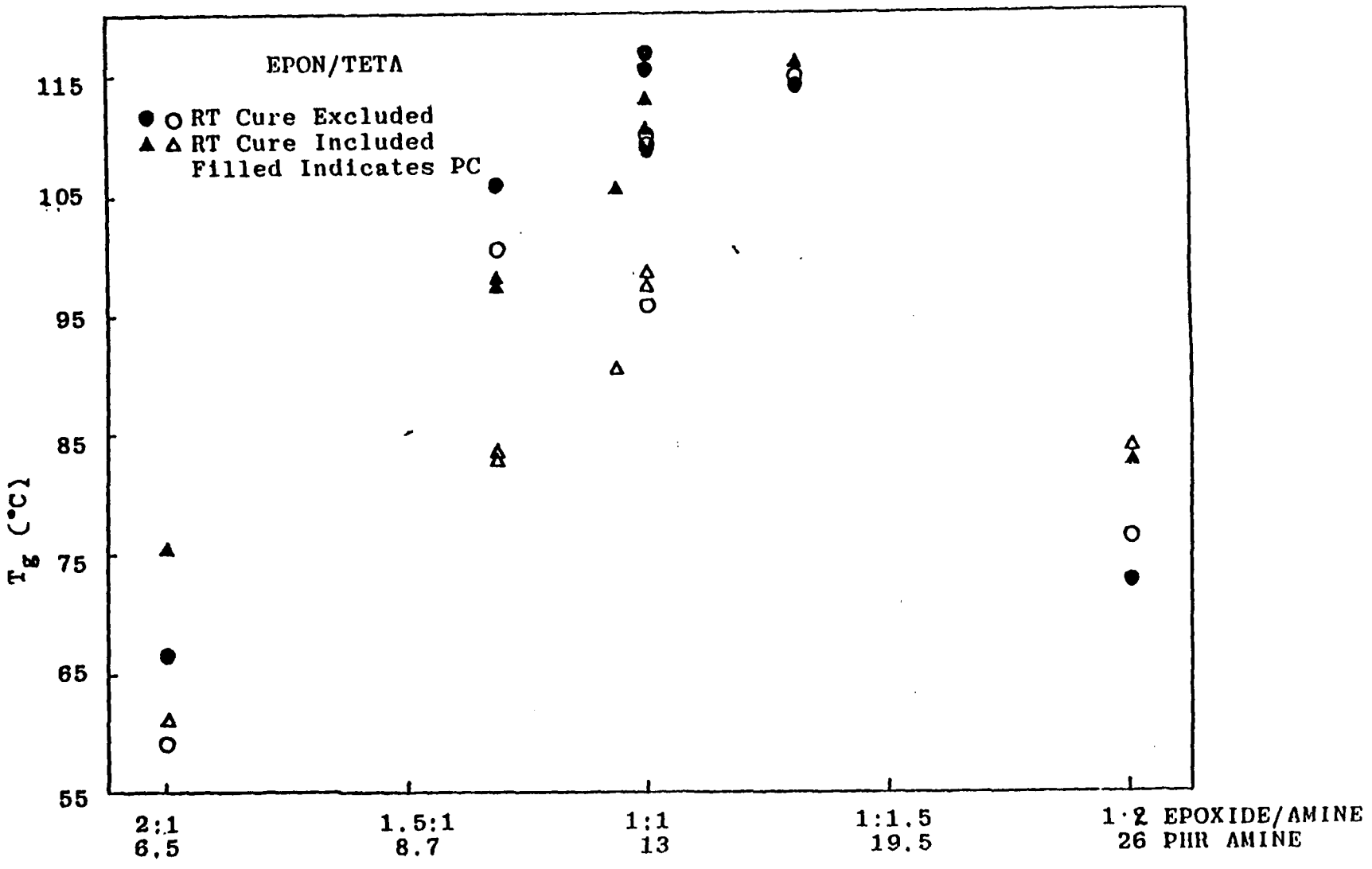
EPON/TETA
● ○ RT Cure Excluded
▲ △ RT Cure Included
Filled Indicates PC
115
105
95
85
75
65
55
T_g (°C)
2:1
6.5
1.5:1
8.7
1:1
13
1:1.5
19.5
1:2 EPOXIDE/AMINE
26 PHR AMINE

Figure 1

TABLE 2

Condition	M_c (grs/mole)
A	2059
K1	580
I2	408
R	905
A^P	1528
$K1^P$	393

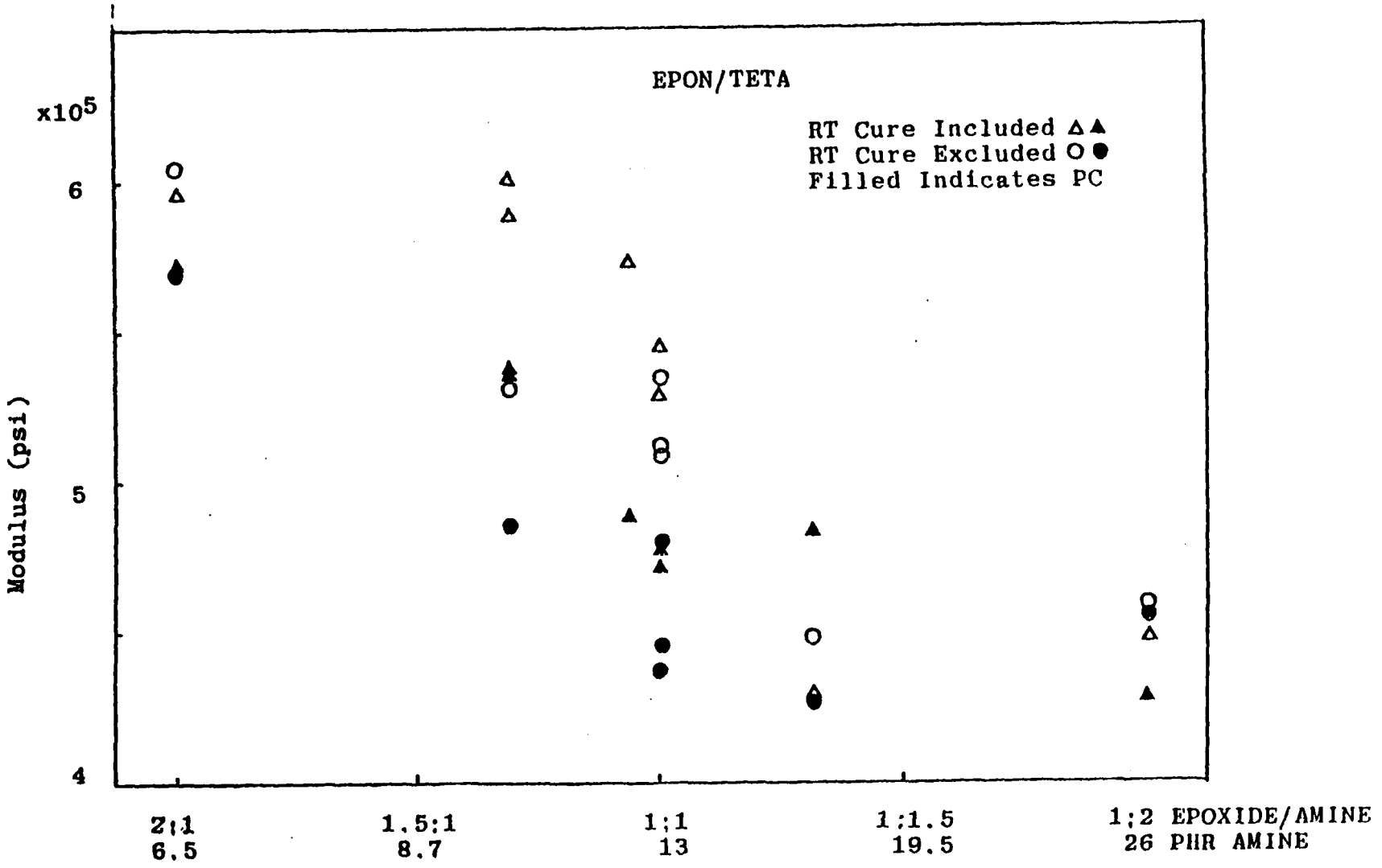

Figure 2 - Flexure modulus (from 4 point bend method) plotted against stoichiometry.

than 50 volume % with an average nodule size of 200-300 Å. The nodules are assumed to be rich in amine and thus have a higher crosslink density than the matrix. This increases their hardness and makes them undeformable.

Figure 2 clearly shows, however, that amine-rich formulations have lower modulus than epoxy-rich or stoichiometric compositions. Hence the arguments based on the occurrence and characteristics of nodules are inconsistent with the data. It has also been shown by SAXS studies that if nodules did exist in the sizes and volume fractions claimed above, then the density difference between the matrix and nodules would be less than 0.1%.

Figure 3 shows a crossplot of the T_g vs modulus data. At both the ends of the curve, T_g drops without a change in modulus. On the left hand side of the figure, the drop occurs for materials which are amine rich (conditions Q, R, Q^P, R^P) and at the other end for the epoxy rich materials (A, B, A^P, B^P). This drop cannot be taken as the formation of the second phase, because if this happened then the modulus would change at constant T_g.

This phenomenon can be explained by a plasticization effect. In the epoxy-rich region, unreacted epoxide plasticizes the matrix; and in the amine-rich region, the high concentration of the flexible curing agent gives the same effect. STEM observations (under Z contrast) on microtomed and stained sections of these specimens show a heterogeneous nature (Figure 4). These were observed only for amine rich formulations, or for stoichiometric compositions which were precured at room temperature. DSC and DMA do not show the presence of two T_g's or shoulders in Tan δ around T_g.

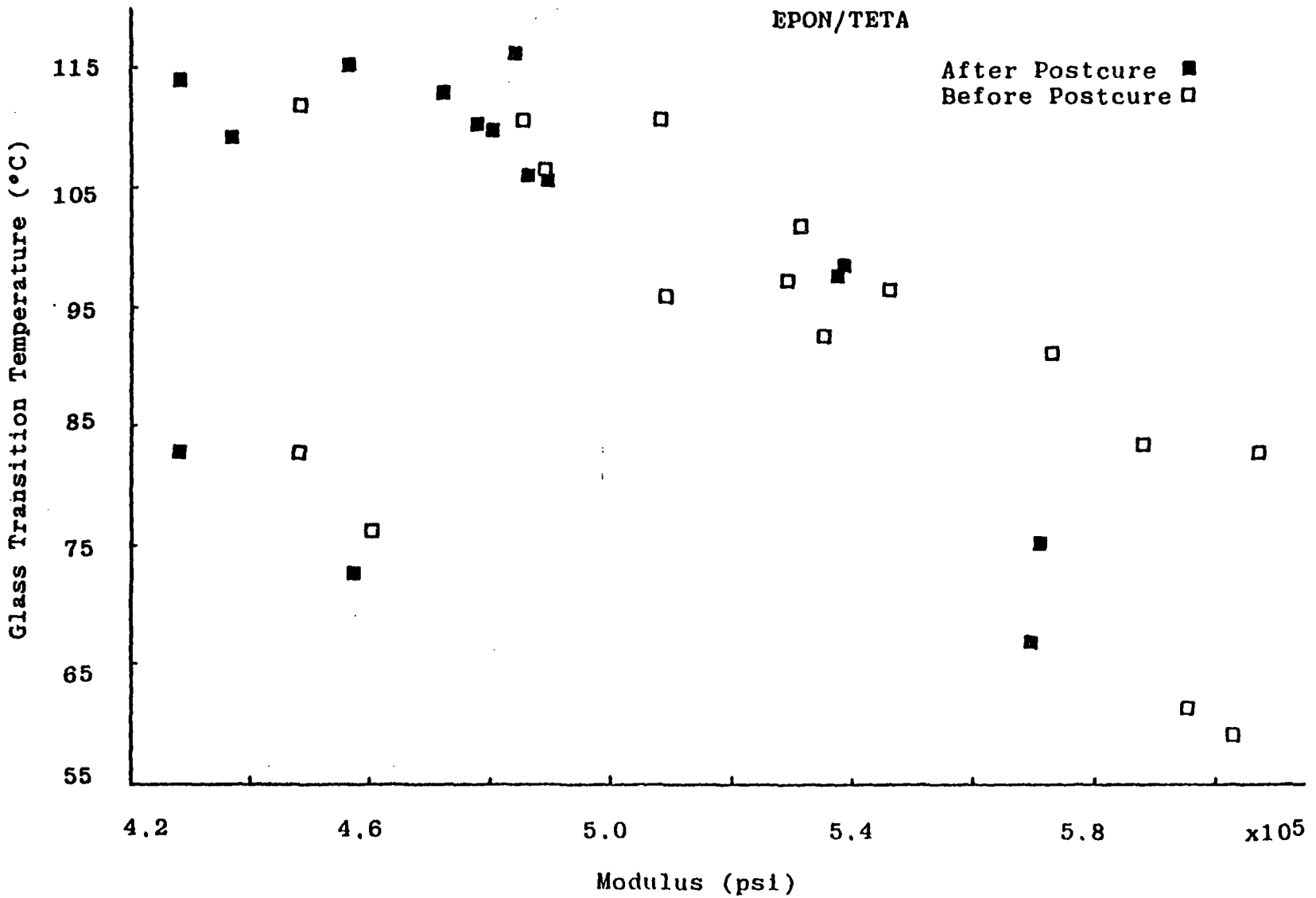

Figure 3 -Onset of Glass Transition Temperature from DSC vs Flexure Modulus.

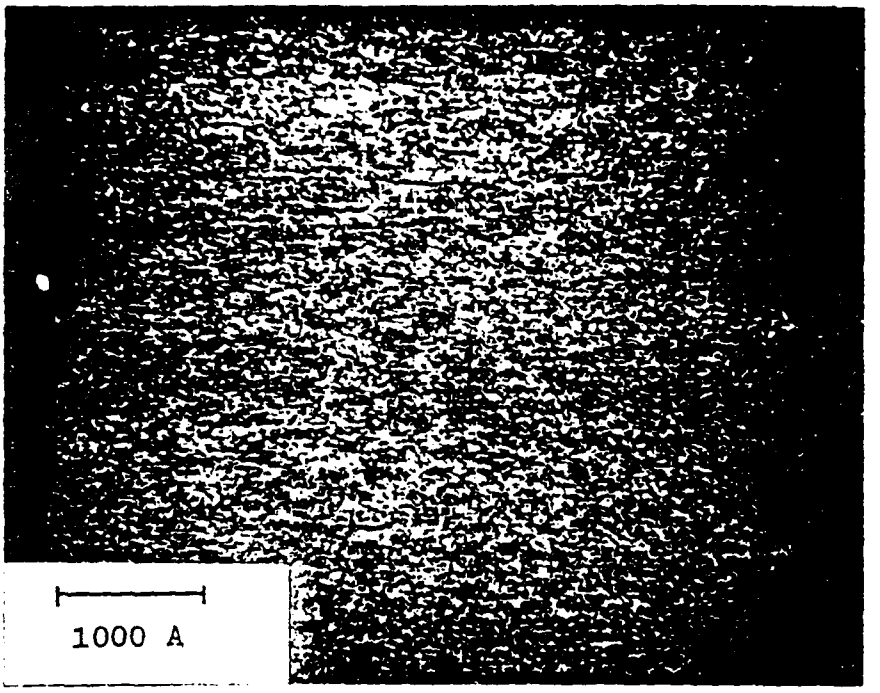

(a)

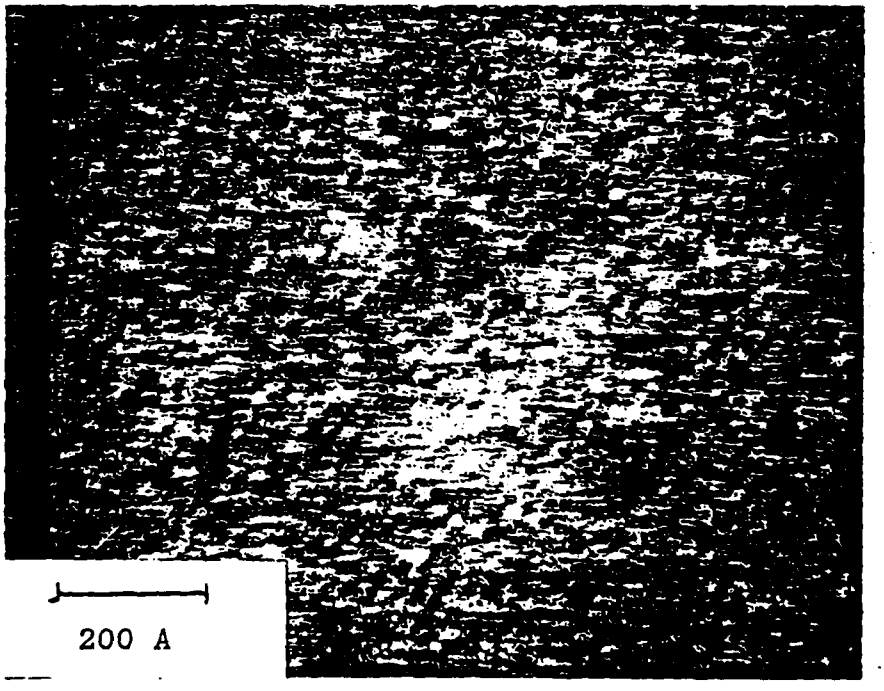

(b)

Figure 4 - Stained STEM micrographs for stoichiometric (condition $L2^P$) formulation. Room temperature cure was given.

It has previously been observed in an aromatic amine/DGEBA epoxy system that the reactivity ratio of the primary and secondary amine (K_1/K_2) is around 5. If this were the case in the present system, then in an amine rich system the primary H will react with the epoxies tending to form long linear chains, which could then precipitate out of the epoxy-rich matrix creating a two-phase system.

It was decided therefore to model the growth of a system with a varying K_1/K_2 and stoichiometry to obtain insight into the types of species formed at various stages of reaction. Figure 5 show the fractions of primary (Q1) amine reacted for different stoichiometries and reactivity ratio r($r=K_1/K_2$) as a function of epoxide consumption. This figure shows the variations only up to the onset of gelation. It should be noted from the figure that the epoxide consumed at the gel point does not vary greatly with changing reactivity ratio.

Table 3 shows the various species that can be generated during the curve of epoxies; and Tables 4 to 9 show the concentrations of the different components at various stages of the reaction. It is seen that at the gel point, in the epoxy rich mixture, most of the contribution to the total extent of reaction comes from highly branched units (N2PIS, N2P2S, N2p3S); whereas in amine-rich mixtures (A/E=2), it comes from the less branched units (N1POS, N1P1S, NOP1S, N2POS). The only branched units contributing substantially to the latter are N2P1S or N1P2S.

With increasing reactivity ratio (K_1/K_2), one observes that in amine rich mixtures the amount of unreacted TETA is reduced and the contribution from N1P2S decreases at the expense of N2P1S (although both have nree of their functionalities reacted).

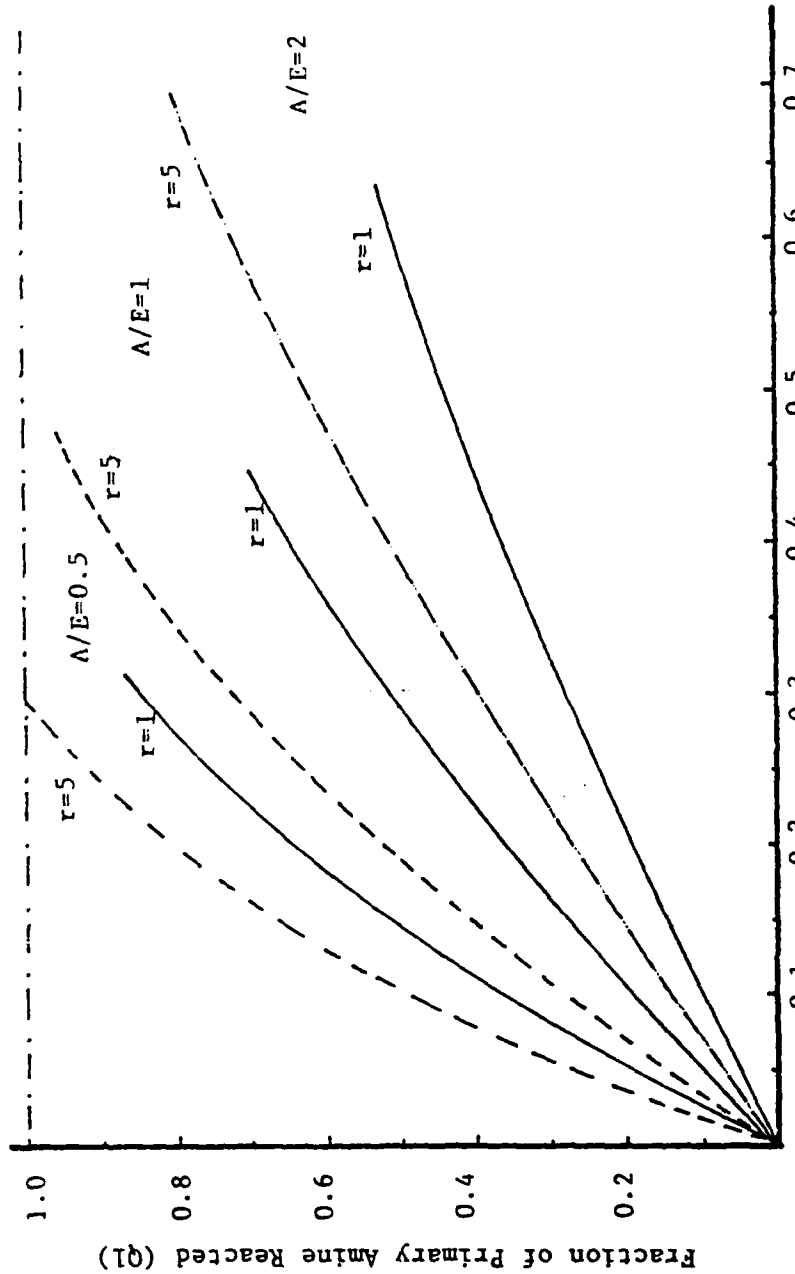

Figure 5 - Fraction of primary amine reacted with increasing consumption of Epoxide. These results are plotted either till gel point or till the primary amine is exhausted.

TABLE 3

Types of Different Species* Generated for TETA.

N0P0S	PSSP	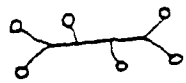
N1P0S	PSSS	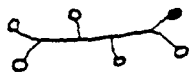
N2P0S	SSSS	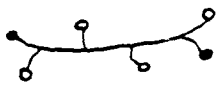
N0P1S	PSTP	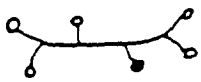
N0P2S	PTTP	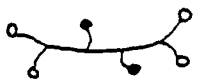
N1P1S	PSTS, PTSS, TSSP	
N1P2S	PTTS, TSTP, TTSP	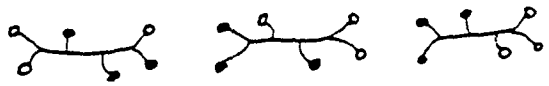
N1P3S	TTTP	
N2P1S	STSS, SSST	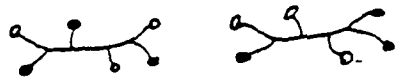
N2P2S	STTS, TSST, TSTS, TTSS	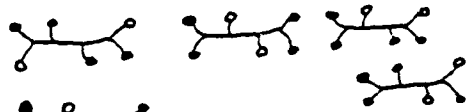
N2P3S	TTTS, TSTT	
N2P4S	TTTT	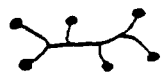

* Specie N0P1S indicates zero primary and one secondary have reacted. This can also be written as PSTP, i.e., the first nitrogen is primary, the second is secondary, the third is tertiary and the last one is also primary. The schematics show TETA molecules, a solid end indicates that it is reacted.

TABLE 4

% of Different Species at Increasing Epoxide Conversion (EPON / TETA)

ρ is the Average Number of Functionalites Reacted for a TETA Molecule

$K_1/K_2 = 1$ AMINE / EPOXIDE = 0.5

Type of Species	% EPOXIDE Conversion		
	8.2	18.4	34.2
N0P0S	34.3	6.4	0.25
N1P0S	26.8	14.9	1.72
N2P0S	5.23	8.65	2.95
N0P1S	13.4	7.44	0.86
N0P2S	1.31	2.16	0.74
N1P1S	13.1	21.6	7.4
N1P2S	2.04	10.05	10.1
N1P3S	0.10	1.46	4.32
N2P1S	3.06	15.1	15.1
N2P2S	0.648	9.49	28.1
N2P3S	0.058	2.54	22.2
N2P4S	0.002	0.247	6.3
ρ =	1.03	2.21	3.79

TABLE 5

% of Different Species at Increasing Epoxide Conversion (EPON / TETA)

ρ is the Average Number of Functionalites Reacted for a TETA Molecule

$K_1/K_2 = 1$ AMINE/EPOXIDE = 1

Type of Species	% EPOXIDE Conversion				
	7.8	16.3	25.8	36.7	44.9
N0P0S	61.4	34.3	16.6	6.4	2.81
N1P0S	20.8	26.8	23.2	14.9	9.14
N2P0S	1.76	5.23	8.1	8.7	7.44
N0P1S	10.4	13.4	11.6	7.43	4.57
N0P2S	0.44	1.31	2.02	2.16	1.86
N1P1S	4.4	13.1	20.2	21.6	18.6
N1P2S	0.3	2.04	5.6	10.05	12.1
N1P3S	0.006	0.10	0.49	1.46	2.46
N2P1S	0.45	3.06	8.4	15.1	18.2
N2P2S	0.041	0.65	3.2	9.49	16.0
N2P3S	0.002	0.058	0.51	2.54	6.01
N2P4S	0	0.002	0.03	0.25	0.82
ρ =	0.47	0.98	1.55	2.21	2.69

TABLE 6

% of Different Species at Increasing Epoxide Conversion (EPON / TETA)

ρ is the Average Number of Functionalites Reacted for a TETA Molecule

$K_1/K_2 = 1$ AMINE/EPOXIDE = 2

Type of Species	% EPOXIDE Conversion						
	7.64	15.6	23.9	32.7	42	62.2	63.2
N0P0S	79.1	61.4	46.5	34.3	16.6	10.72	10.22
N1P0S	12.6	20.8	25.3	26.8	23.2	19.33	18.9
N2P0S	0.5	1.76	3.44	5.23	8.08	8.72	8.74
N0P1S	6.29	10.4	12.7	13.4	11.6	9.67	9.45
N0P2S	0.125	0.44	0.86	1.31	2.02	2.18	2.19
N1P1S	1.25	4.4	8.6	13.1	20.2	21.8	21.9
N1P2S	0.04	0.3	0.94	2.04	5.63	7.86	8.09
N1P3S	0	0.006	0.032	0.10	0.49	0.886	0.935
N2P1S	0.06	0.447	1.4	3.06	8.44	11.8	12.13
N2P2S	0.03	0.041	0.207	0.65	3.19	5.76	6.08
N2P3S	0	0.002	0.013	0.058	0.512	1.20	1.3
N2P4S	0	0	0	0.002	0.03	0.09	0.1
ρ =	0.23	0.47	0.73	0.98	1.55	1.87	1.90

TABLE 7

% of Different Species at Increasing Epoxide Conversion*(EPON / TETA)

ρ is the Average Number of Functionalites Reacted for a TETA Molecule

$K_1/K_2 = 5$ AMINE/EPOXIDE = 0.5

Type of Species	% of EPOXIDE Conversion			
	5.7	12	20.6	29.7
N0P0S	45.6	13.3	0.63	0.001
N1P0S	38.4	37.9	9.7	0.168
N2P0S	8.07	27	37.6	13.37
N0P1S	3.31	2.56	0.33	0.001
N0P2S	0.06	0.122	0.042	0
N1P1S	3.52	9.32	6.66	0.344
N1P2S	0.104	0.74	1.49	0.232
N1P3S	0.001	0.019	0.109	0.032
N2P1S	0.89	8.08	32	34.9
N2P2S	0.036	0.88	10	34
N2P3S	0.001	0.042	1.38	14.6
N2P4S	0	0.001	0.07	2.34
ρ =	0.68	1.45	2.47	3.56

* At 29.7% of Epoxide conversion, all primary amine was exhausted and the Gel point was not reached ($\alpha = 0.84$).

TABLE 8

% of Different Species at Increasing Epoxide Conversion (EPON / TETA)

ρ is the Average Number of Functionalites Reacted for a TETA Molecule

$K_1/K_2 = 5$ AMINE/EPOXIDE = 1

Type of Species	% of EPOXIDE Conversion						
	5.6	11.3	17.4	23.9	31.3	41.1	47.4
N0P0S	69.9	45.6	26.8	13.32	4.74	0.631	0.10
N1P0S	24.5	38.4	42.5	37.9	26.1	9.74	3.5
N2P0S	2.14	8.1	16.8	27	36	37.6	31.1
N0P1S	2.3	3.31	3.31	2.56	1.41	0.33	0.073
N0P2S	0.02	0.06	0.102	0.123	0.105	0.042	0.013
N1P1S	1.01	3.52	6.65	9.32	10.1	6.66	3.48
N1P2S	0.013	0.103	0.34	0.74	1.26	1.49	1.13
N1P3S	0	0.001	0.005	0.019	0.051	0.109	0.121
N2P1S	0.106	0.89	3.19	8.08	17.04	32	38.7
N2P2S	0.002	0.036	0.22	0.884	2.95	10.0	17.9
N2P3S	0	0.001	0.001	0.042	0.222	1.38	3.63
N2P4S	0	0	0	0.001	0.006	0.07	0.273
ρ =	0.34	0.68	1.04	1.44	1.89	2.47	2.84

TABLE 9

% of Different Species at Increasing Epoxide Conversion (EPON / TETA)

ρ is the Average Number of Functionalites Reacted for a TETA Molecule

$K_1/K_2 = 5$ AMINE/EPOXIDE = 2

Type of Species	% EPOXIDE Conversion						
	5.54	11.2	16.9	28.7	41.2	54.9	69
N0P0S	84.2	69.9	57.1	35.6	19.4	8.44	2.73
N1P0S	13.6	24.5	32.7	41.6	41.2	32.8	20.4
N2P0S	0.55	2.14	4.68	12.2	21.9	31.9	38.1
N0P1S	1.32	2.29	2.95	3.4	3.01	2.01	0.97
N0P2S	0.005	0.019	0.038	0.082	0.12	0.119	0.086
N1P1S	0.266	1.01	2.13	5.07	8.12	10.04	9.45
N1P2S	0.002	0.013	0.044	0.199	0.517	0.997	1.43
N1P3S	0	0	0	0.002	0.010	0.032	0.069
N2P1S	0.013	0.11	0.367	1.793	5.23	11.94	21.8
N2P2S	0	0.002	0.010	0.096	0.457	1.64	4.57
N2P3S	0	0	0	0.002	0.017	0.097	0.417
N2P4S	0	0	0	0	0	0.002	0.014
ρ =	0.17	0.34	0.51	0.86	1.24	1.65	2.07

To examine whether such results for large r (>2) in amine-rich systems would lead to the formation of long linear polymer chains (which would then precipitate to give a second phase), further calculations were carried out (see appendix for details of calculations), with the results shown in Tables 10 and 11. These tables lists the % probability for the formation of diads and triads. The type of triad listed is of the type which will lead to longer polymeric species. The probability of the formation of this triad increases appreciably at r = 5 in amine rich formulations. In the limit that r = 2, the reactivity differences between primary and secondary amines will not cause an appreciable change in the nature of the species. However, it may help explain the inhomogeneity of amine rich mixtures.

To consider this, it is useful to evaluate the difference in the solubility parameters required for precipitation. It has been argued that precipitation occurs when Δ is greater than 5

$$\Delta = \sqrt{((\delta_{v1} - \delta_{v2})^2 + (\delta_{h1} - \delta_{h2})^2)} \qquad (2)$$

for polymeric species, and greater than 10 for monomeric species. δ_v and δ_h are the contributions to the solubility parameters due to dispersive polar forces and hydrogen bonding respectively. Subscripts 1 & 2 refer to the precipitating species and the matrix component. Table 12 lists values of these parameters for different species. It can be argued that the polymeric species shown in Table 13 has a Δ of 9.28 (as compared to DGEBA) which is more than 5 hence it would precipitate. The reference point has been taken as DGEBA because only 43% of epoxide had reacted at gelation; therefore an assumption was made that a sea of unreacted epoxy remained.

TABLE 10

Percentage Probability for the Formation of Triads* as the Function of Stoichiometry and K_1/K_2 at different Stages of Reaction

	% Primary Amine Reacted								
	A/E = 2			A/E = 1			A/E = 0.5		
K_1/K_2	15	30	Gel	30%	60%	Gel	30%	60%	Gel
1	8.99	15.64	8.47	7.81	2.71	1.08	3.9	1.36	0.022
2	9.09	19.93	10.4	9.97	6.95	0.94	4.99	3.46	0
5	8.9	22.3	7.12	11.14	11.46	0.12	5.57	5.74	-

* 

TABLE 11

Percentage Probability for the Formation of Diads* as the Function of Stoichiometry and K_1/K_2 at Different Stages of Reaction

	% Primary Amine Reacted								
	A/E = 2			A/E = 1			A/E = 0.5		
K_1/K_2	15	30	Gel	30	60	Gel	30	60	Gel
1	26.3	27.0	10.4	33.6	14.1	7.56	36.9	18.2	1.7
2	24.9	30.2	9.4	35.7	22.5	5.75	38.4	27.2	0.6
5	23.8	32.2	6.64	37.0	30.8	1.9	39.3	35.6	-

* 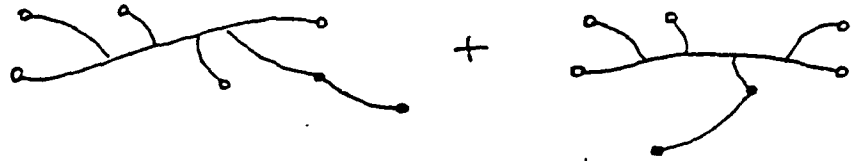

TABLE 12

Solubility* Parameters of Different Species $((J/cm^3)^{1/2})$.

Type of Species	δ_d	δ_p	δ_v	δ_h
Triad	16.44	1.743	16.53	11.61
Primary Diad	17.3	2.04	17.42	10.06
Secondary Diad	17.25	2.60	17.44	10.81
DGEBA	17.21	0.64	17.22	1.72

* $\delta_v = \sqrt{\delta_d^2 + \delta_p^2}$

Subscripts d, p, and h refer respectively to dispersive, polar and hydrogen bonding contributions to the solubility parameter.

TABLE 13

Difference in Solubility* (Δ) for Different Species

Species 1	Species 2		
	DGEBA	Diad Primary	Diad Secondary
DGEBA	0	8.34	9.09
Diad Secondary	9.09	0.75	0
Diad Primary	8.34	0	0.75
Triad	9.91	1.79	1.21

* $\Delta = \sqrt{(\delta_{v1} - \delta_{v2})^2 + (\delta_{h1} - \delta_{h2})^2}$

From a probabilistic calculation, the completely undreacted molecules of epoxide will be only $(1-43)^2$--i.e., 32%. At gelation (gelation occurs at a different value in amine-rich system here due to a different stoichiometry), completely uncreacted epoxy is present in only a small quantity which cannot form the matrix (Table 14). The matrix consists of diads and other species which have solubility parameters (Tables 12, 13) intermediate between those of unreacted epoxy and the triads (or the higher polymeric species that are formed). Considering one step before gelation, where the phase separation can take place without being hindered sterically, one can consider that the diads (wnich are still soluble in epoxy) act as buffers to keep the triads in solution. The difference in solubility parameter between the epoxy and the triads can be reduced; and it is concluded that phase separation giving rise to a large fraction (50 volume % or more) of heterogeneities cannot be explained in this way.

TABLE 14

Various Kinds of Epoxide Present (%) at Different Stages of Reaction as a Function of Stoichiometry and K_1/K_2

K_1/K_2	Type of Species*	% of Primary Amine Reacted								
		A/E = 2			A/E = 1			A/E = 0.5		
		Gel	30	15	[illegible]	60	30	Gel	60	30
1	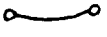	13.5	5.3	71.2	30.4	40	70	46.8	66.6	84
		46.5	44	26.3	49.5	46.5	27.3	43.2	30	15
		40	10.7	2.43	20.1	13.5	2.7	10	34	1.0
2	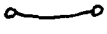	12.0	53.9	75.9	29.4	50	75.2	46	72.9	87
	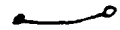	45.3	39	22.4	49.6	41.4	23.1	43.6	25	12.4
		42.7	7.1	1.65	21	8.6	1.77	10.3	2.1	0.44
5	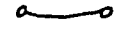	9.62	59.7	78.0	27.7	57.9	78.6	-	77.5	89
		42.8	35.1	19.8	49.9	36.4	20.1	-	21.1	10.7
		47.6	52	1.25	22.4	5.73	1.29	-	14.3	0.3

* A solid end indicates reacted.  shows an epoxide molecule with one end reacted.

III. CERAMICS FROM ORGANO-METALLIC PRECURSORS

Our investigations of the conversion of organo-metallic precursors to ceramics have directed attention to five principal areas. These were:

1. Investigation of hydrolysis and condensation kinetics of tetraethylorthosilicate (TEOS), an important precursor for many glasses and ceramics;

2. Exploration of the competition between crystallization and viscous sintering, to determine the conditions under which dense glassy bodies or coatings can be obtained;

3. Investigation of the hydrolysis and condensation of tantalum ethoxide to form coatings of tantalum oxide;

4. Initial exploration of organic modified oxides as novel coatings and bulk materials; and

5. Exploration of the conversion of aluminum alkoxides, most notably aluminum sec butoxide, to aluminum oxide.

Progress in the first two of these areas will be described in the present report; progress in the last three will be deferred to a later date.

A. Hydrolysis and Condensation Kinetics of Tetraethylorthosilicate (TEOS)

The sol-gel process for preparing glasses and crystalline ceramics has many potential advantages over conventional melt or powder processing techniques. Among these, four have specific relevance to the present work. These are: (1) the high level of chemical homogeneity which is attainable; (2) the possibility of relatively low-temperature processing; (3) the ability to tailor composition, structure and properties; and (4) the ease and cost effectiveness with which coatings can be applied. These advantages can, however, readily be lost if the proper chemistry and

processing conditions are not chosen. For example, if the hydrolysis and condensation rate of one of the components in a multicomponent system is much faster than the others, one oxide or hydroxide may precipitate out of the solution (upon the addition of water) before the other has begun to react.

Data of several investigators have indicated that in the case of tetraethylorthosilicate (TEOS), the rate of disappearance of water can be described with simple first order kinetics. Assuming this to be the case, the absolute reaction rate was precisely determined. Rates for other alkoxides could theoretically be measured and compared, and calculations could be made as to how much water should be added and when it should be added to maximize the number of M_1-O-M_2 bridges. Here M_1 and M_2 are metal cations (Si, Al, etc.) and O is oxygen. Pursuing this lead, investigations were undertaken of the kinetic behavior of TEOS in ethanol and water using infrared spectroscopy to measure the concentration of water as a function of time, using the 1640 cm^{-1} band.

All the infra-red data were taken on a Perkin Elmer model 297 using a calcium fluoride cell of nominal pathlength 0.01 mm. The absolute pathlength was not calibrated before each run, so that absorbance cannot be converted directly to concentration. As a result, the data cannot be compared from run to run except where the cell was not taken apart between. However, each experiment may be analyzed on a relative concentration basis. Fortunately, in determining the order of the reaction, absolute concentration does not matter, only the relative rate of change as discussed below.

The form of the data for all starting compositions appeared similar when the log of the relative rate was plotted against the log of the absorbance. Figure 6 shows a representative plot for the 1:1:4 starting

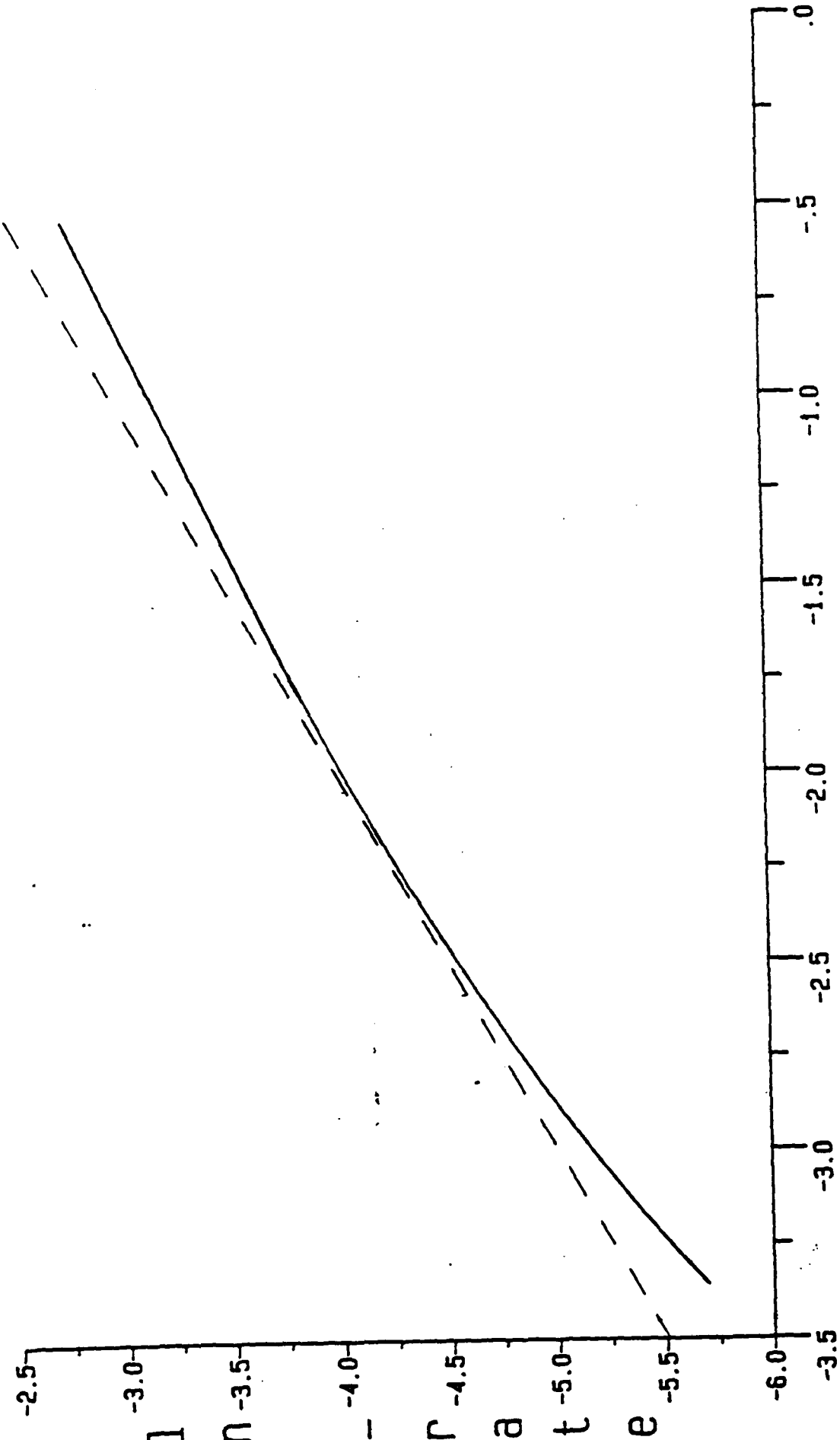
1:1:4 Apparent Order
ln rate
ln conc.
-2.5
-3.0
-3.5
-4.0
-4.5
-5.0
-5.5
-6.0
.0
-.5
-1.0
-1.5
-2.0
-2.5
-3.0
-3.5

Figure 6

composition (the numbers represent the molar ratios of water to TEOS to ethanol). As was the case for all experiments run, the acid concentration of the entire solution was 10^{-2} normal HCl. When these data are compared with those obtained on the 1:2:4 and 1:4:4 starting compositions (Figures 7 and 8), it can be seen that the initial apparent orders of the reaction decrease with increasing water concentration and even become negative in the 1:4:4 case. All three systems show significant deviation from first order kinetics throughout most of the course of the reaction.

In an effort to determine if starting with very clean components alters the apparent order of the kinetics, several experiments on the 1:1:4 starting composition were made. As illustrated in Figure 9a, there was little difference between TEOS used as-received compared with the same material which had been freshly distilled, when both were hydrolysed with deionized water and Acculute HCl was used as the acid source. There was no noticeable difference when 18 megaohm water was used for hydrolysis in conjunction with Acculute. Finally, silicon tetrachloride was added to ethanol to generate the HCl; and when this was used in conjunction with 18 megaohm water, the initial apparent order fell much closer to unity (Figure 9b). This experiment was run twice; and the results point out how much variation might be expected in such data. This entire series of experiments was run without dismantling the cell, so that the results can be compared quantitatively.

Data obtained under a range of conditions were analyzed in terms of the principles of chemical kinetics. In these terms, the rate of disappearance of one of the species in a reaction can be related to the concentrations of the reactants. For the reaction shown as Equation (3), the rate of

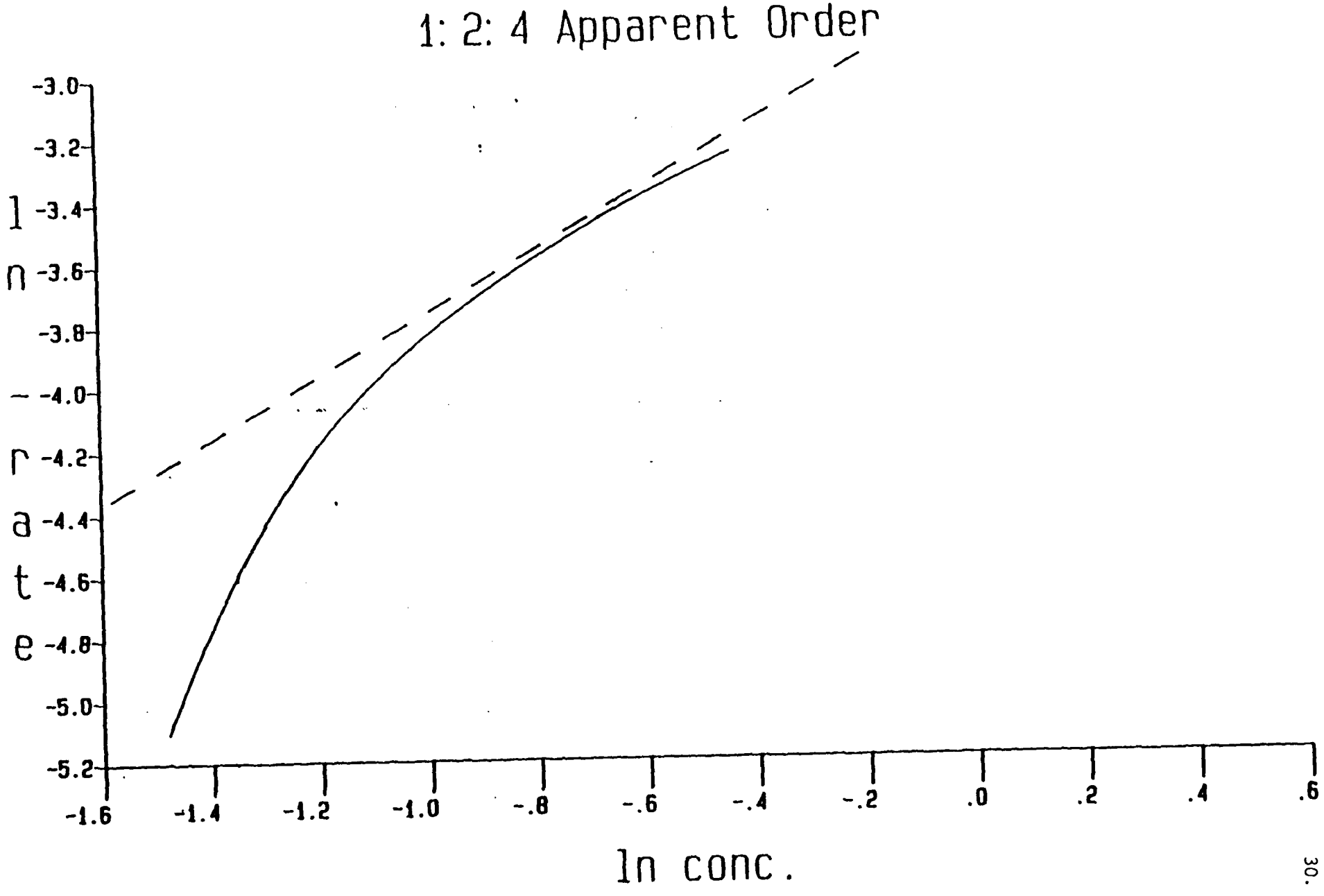
1: 2: 4 Apparent Order
-3.0
-3.2
-3.4
-3.6
-3.8
-4.0
-4.2
-4.4
-4.6
-4.8
-5.0
-5.2
ln rate
-1.6
-1.4
-1.2
-1.0
-.8
-.6
-.4
-.2
.0
.2
.4
.6
ln conc.

Figure 7

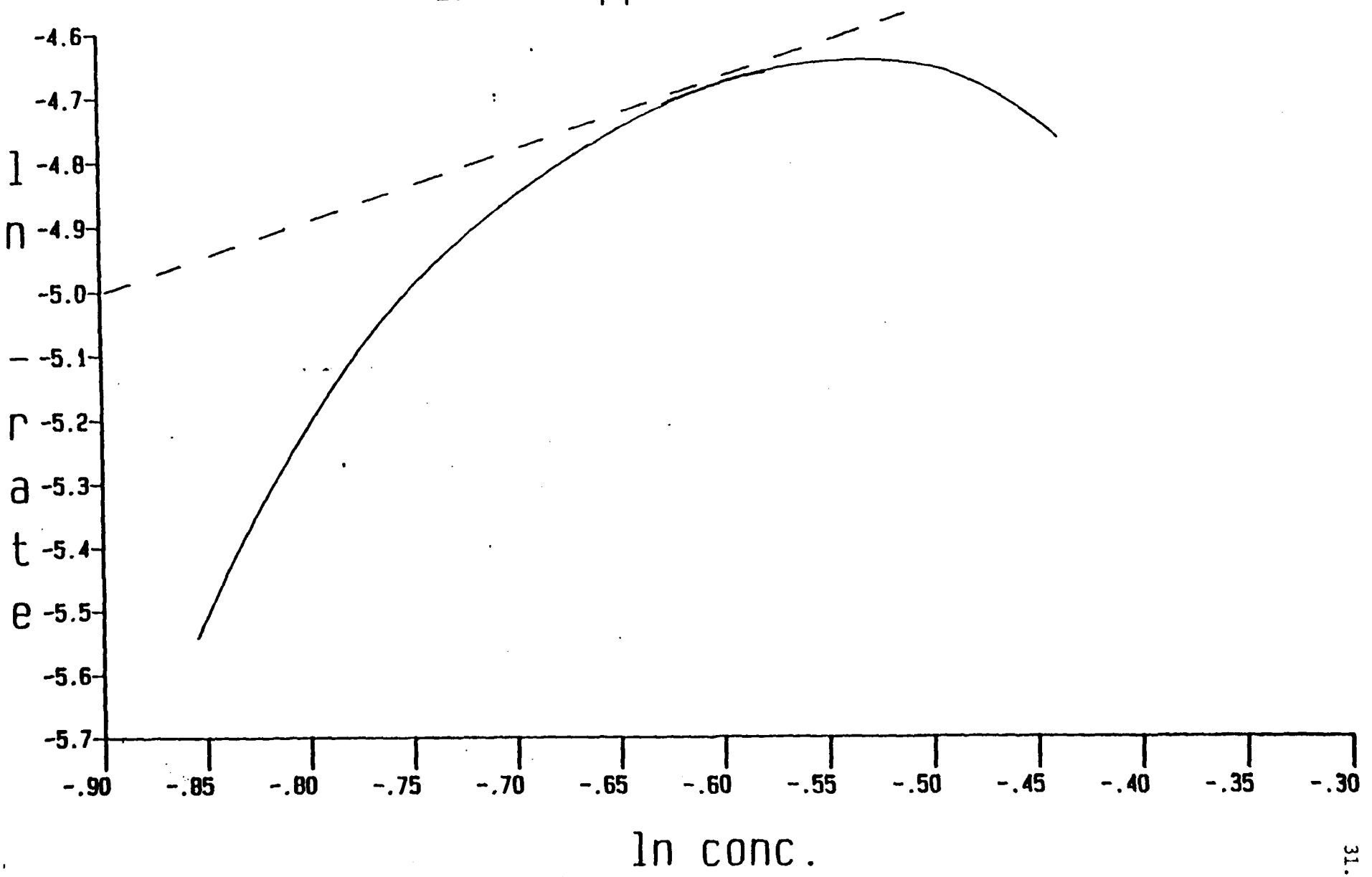
1: 4: 4 Apparent Order
-4.6
-4.7
-4.8
-4.9
-5.0
-5.1
-5.2
-5.3
-5.4
-5.5
-5.6
-5.7
ln rate
-.90
-.85
-.80
-.75
-.70
-.65
-.60
-.55
-.50
-.45
-.40
-.35
-.30
ln conc.

Figure 8

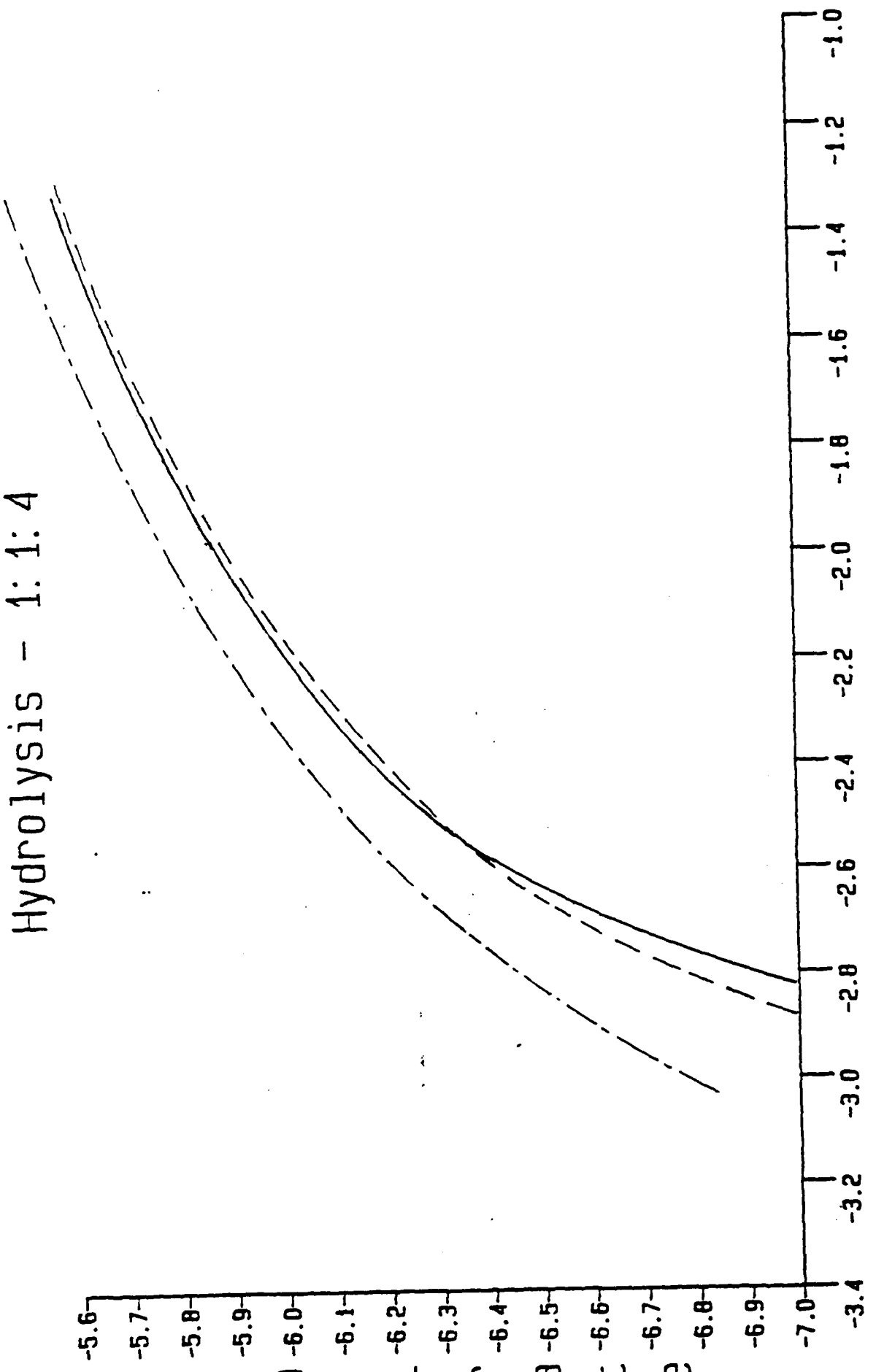
Hydrolysis - 1:1:4
ln rate
-5.6
-5.7
-5.8
-5.9
-6.0
-6.1
-6.2
-6.3
-6.4
-6.5
-6.6
-6.7
-6.8
-6.9
-7.0
-3.4
-3.2
-3.0
-2.8
-2.6
-2.4
-2.2
-2.0
-1.8
-1.6
-1.4
-1.2
-1.0
ln conc.

Figure 9a

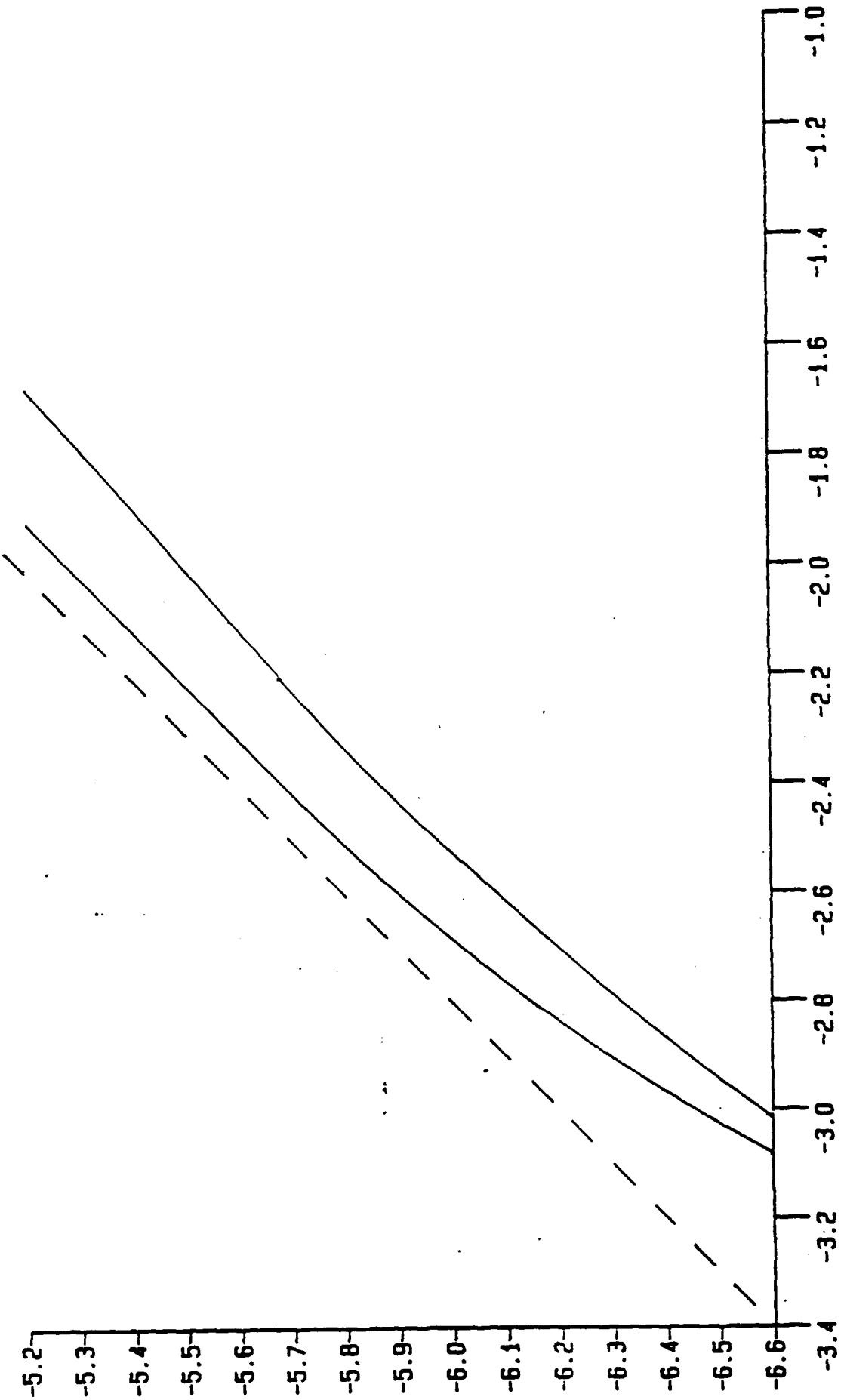
Ultra-Clean Hydrolysis
ln rate
-5.2
-5.3
-5.4
-5.5
-5.6
-5.7
-5.8
-5.9
-6.0
-6.1
-6.2
-6.3
-6.4
-6.5
-6.6
-3.4
-3.2
-3.0
-2.8
-2.6
-2.4
-2.2
-2.0
-1.8
-1.6
-1.4
-1.2
-1.0
ln conc.

Figure 9b

disappearance of A can be expressed as Equation (4)

$$A + B \rightarrow C + D \tag{3}$$

$$-\frac{d[A]}{dt} = K_f[A]^m[B]^n \tag{4}$$

Here m and n are the orders of the reaction with respect to each component. An important assumption made here is that the reaction is irreversible. If this were not the case, the rate of production of A using the back reaction can be shown as Equation (5):

$$\frac{d[A]}{dt} = K_b[C]^k[D]^l \tag{5}$$

The total rate of change of the concentration is the sum of these two equations. In these equations, K_f and K_b are reaction rate constants for the forward and back reactions, respectively. They are independent of composition, but are functions of temperature.

In the standard analysis, the concentration of A is plotted against time, and a polynomial curve is fit to the data. The derivative is taken, and the log of this is plotted against the log of the concentration. In most cases, a straight line results whose slope is equal to m, the order of the reaction with respect to A. This is only true, however, if the concentration of B is relatively constant. If this is not the case, a more complex form is followed.

Reaction rate data are usually taken with all components except one in vast excess in order to eliminate the aforementioned problem. In our case, however, we are working in a composition range where the initial concentrations of A and B are comparable. In the case where the initial concentrations are identical, Equation (4) can be reduced to Equation (6):

$$-\frac{d[A]}{dt} = K_f[A]^{m+n} \tag{6}$$

If the reaction is actually first order in both components, it will appear second order with respect to A (due to B varying at the same rate as A). For the sake of simplicity, the orders of reaction with respect to each component will be assumed to be unity from this point on, as is assumed to be the case for TEOS.

Upon separation of the variables and integrating, the concentration as a function of time is given as Equation (7):

$$[A] = \frac{[A]_o}{K_f t[A]_o + 1} \tag{7}$$

For an excess of B, the derivation is slightly more difficult, and has been outlined below for the initial concentrations [B] = 4[A].

Equation (3) shows that A and B combine in equimolar quantities, so that for the initial conditions of [B] = 4[A], there is a threefold excess of B. If x is the concentration of A as a function of time, then the concentration of B equals x + 3. Substituting this expression into Equation (4), Equation (8) is generated.

$$-\frac{dx}{dt} = K_f x(3+x) \tag{8}$$

Separating the variables, one obtains Equation (9):

$$\frac{dx}{x(3+x)} = -K_f dt \tag{9}$$

Setting up the definite integrals of x going from $[A_o]$ to [A] and time going from 0 to t, one obtains Equation (10):

$$\frac{1}{3}\left[\ln\left(\frac{x}{x+3}\right) - \ln\left(\frac{1}{4}\right)\right] = -K_f t \tag{10}$$

Following the same procedure for the general initial case [B] = [A]+y, one obtains the general form:

$$t = -\frac{1}{yK_f} \ln \frac{[A](y+[A_o])}{[A_o](y+[A])} \qquad (11)$$

In order to examine the apparent order of the reaction as evidenced by the disappearance of water, it is necessary to plot the log of the rate of disappearance against the log of the concentration and measure the slope. The method described below is roundabout, but parallels the analysis of the computer simulations of hydrolysis which we have carried out. Using Equation (11), a table of water concentration vs. time was generated. These data were then normalized by scaling the initial concentration to 1 and choosing values for K_f so that all curves passed through another common point. This procedure makes the A to B ratio the only variable.

At this point, a plot of the normalized concentration vs. normalized time was generated (Figure 10). The derivatives of the curves were calculated and $\ln(-\frac{d[A]}{dt})$ was plotted against ln[A] (Figure 11). Several features of this graph should be noted. An initial ratio of B to A of 16 is needed for the initial part of the reaction to appear to be first order in A. As this ratio decreases, the apparent order increases. However, the initial apparent order increases faster than the apparent order during the latter stages of the reaction. This results in a curve that is initially steep, and approaches a slope of unity as the reaction proceeds. However, when A and B are present in stoichiometric amounts, the slope is constant at 2. This shows that the apparent order for even the initial part of the reaction can vary from one to two, depending on the initial concentration rate of A to B.

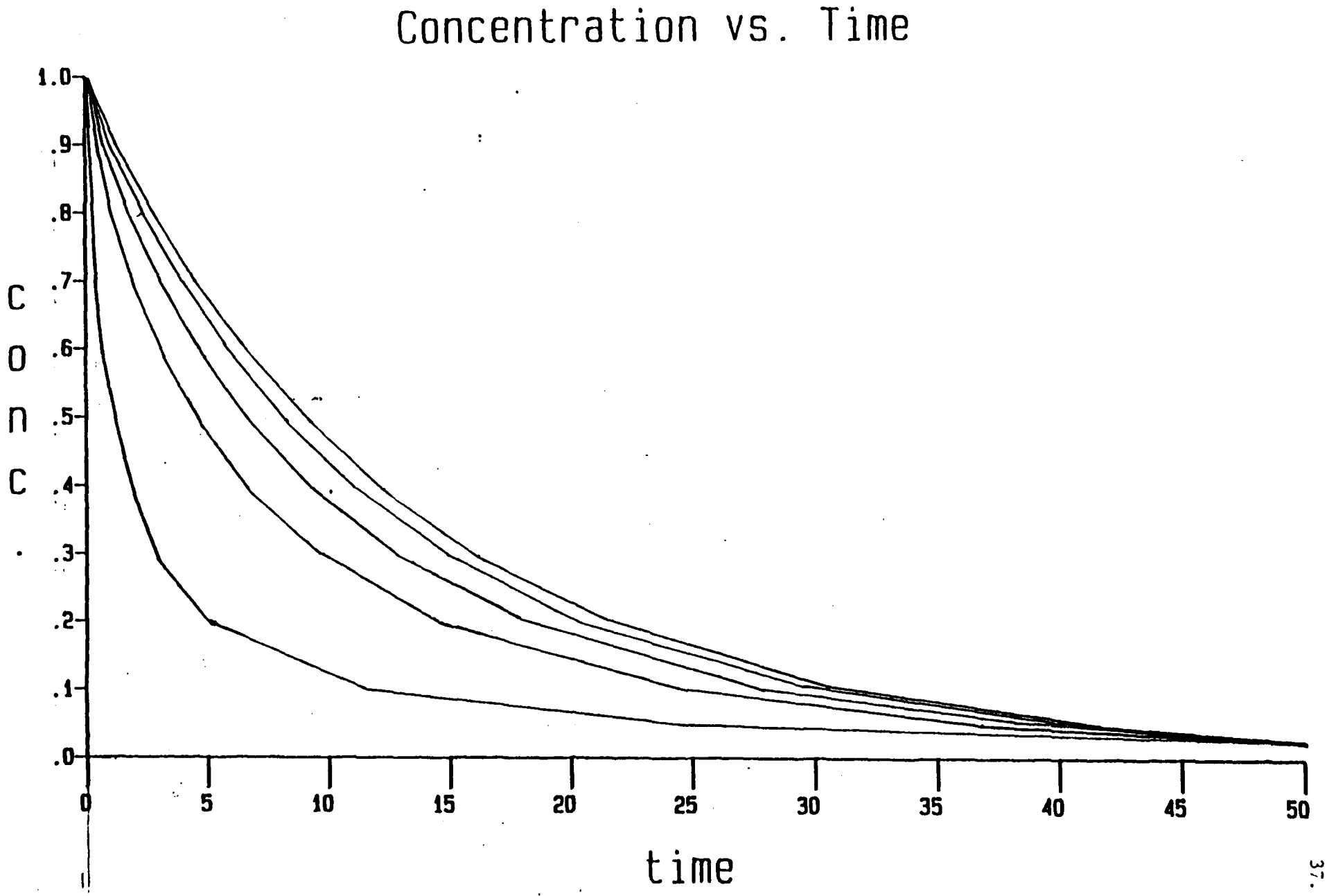
Concentration vs. Time
conc.
1.0
.9
.8
.7
.6
.5
.4
.3
.2
.1
.0
0
5
10
15
20
25
30
35
40
45
50
time

Figure 10

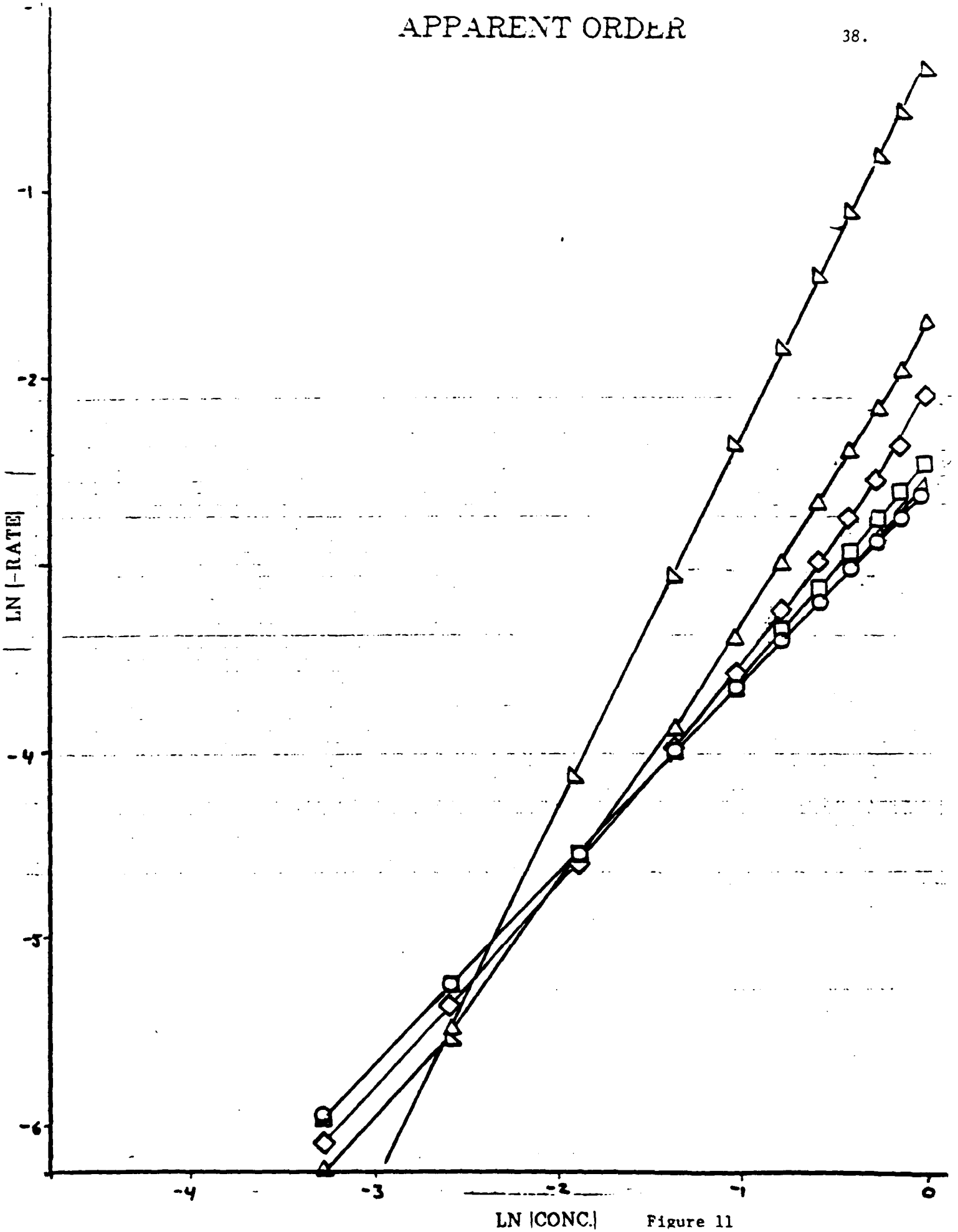

Figure 11

Up to now, we have discussed a system which undergoes only one possible reaction which is first order and irreversible. In the case of TEOS, these assumptions are incorrect. Water is a reactant in all four of the possible hydrolysis reactions and half of the many condensation reactions, so even if we maintain the irreversibility criterion, the behavior of the water concentration as a function of time may be quite complex.

Consider only two possible reactions which use a common reactant, as indicated in Equations (12) and (13):

$$A + B \rightarrow C + D \tag{12}$$

$$A + C \rightarrow E + D \tag{13}$$

These two reactions correspond to the first two hydrolysis reactions of TEOS, where A is water, B is TEOS, C is triethoxysilanol, D is ethanol, and E is diethoxysilanediol. If we were able to inhibit one of these reactions while allowing the other to proceed, we would find first order kinetics for the disappearance of water when we start with a vast excess of silane. If we were to assume that the rate of the second reaction is higher than the first (as is predicted for TEOS) while still occurring independently, we would expect results similar to Figure 12.

For the case of TEOS, these two reactions are not separable. However, when the reactions are initiated, since reactants for only the first reaction are present, the instantaneous rate of the reaction would lie on the lower of the two lines in Figure 7. As soon as the first product appears, the rate of water consumption may deviate from this line. For the case where B is present in vast excess, if the rate of the second reaction is infinitely faster than the first, we would expect to see an overall rate of water

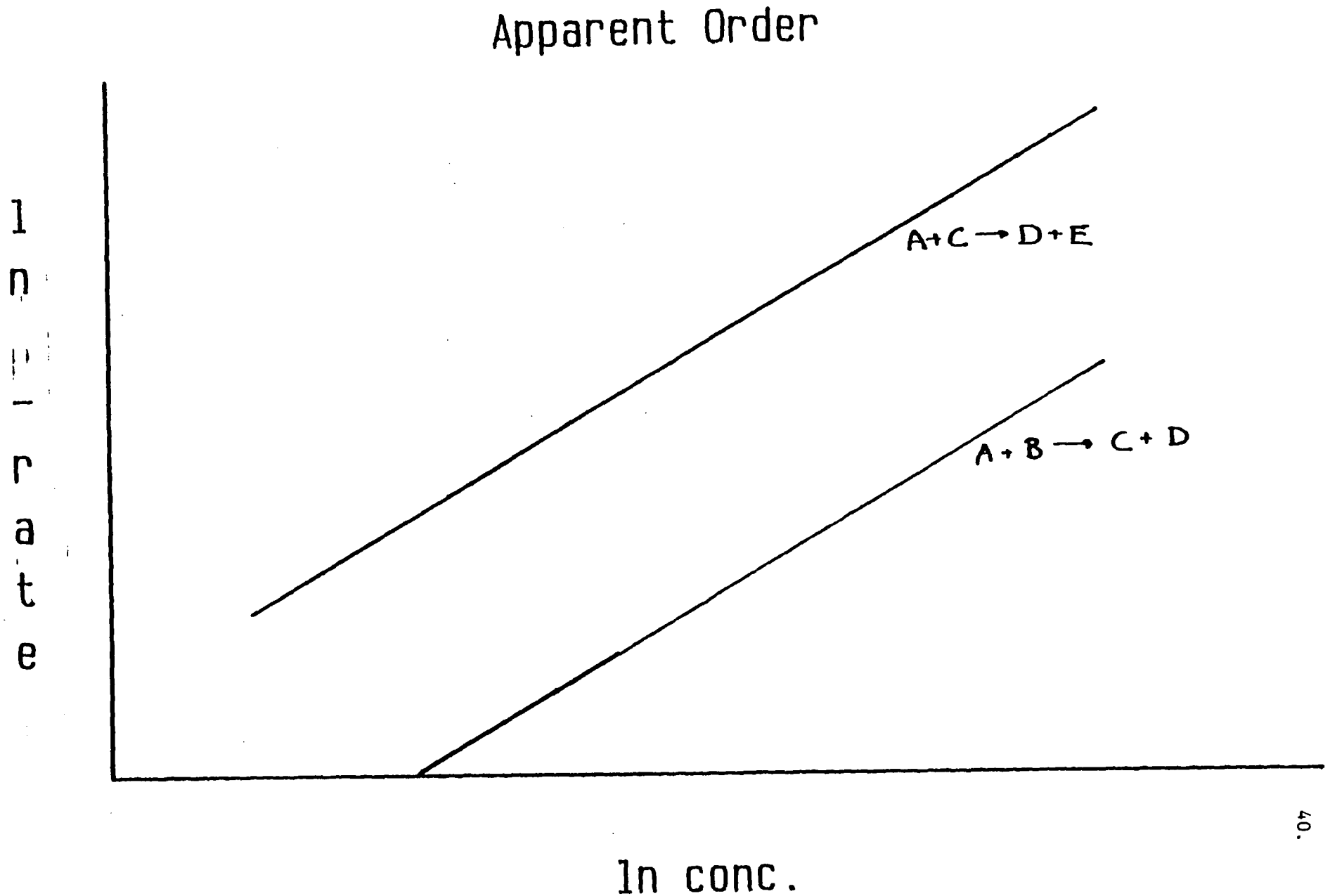

Figure 12

consumption double that of the first reaction. This is because as soon as a molecule of B reacts, a molecule of C will be produced which will instantaneously consume another water molecule. This will be reflected by a line that still has a slope of unity, but is displaced upward by a factor of ln(2). In the other extreme, we have already said that if C does not react, the overall rate will follow the lower line.

It has been mentioned earlier that at least a sixteen-fold excess of B is needed for the slope of the ln(-rate) vs. ln(concentration) to be unity. If the previous analysis is carried out in a regime where the starting B to A ratio is only 8, the results change. As we have seen before, if C does not react, the slope of the initial curve will be slightly greater than unity. If the reaction rates were the same, we would have a situation equivalent to having a sixteen-fold excess of B where C does not react. And, as before, if C reacts instantaneously we would expect a curve parallel to the original one, displaced higher by a factor of ln(2). For the case where C reacts faster than B but is not instantaneous, we would expect the resulting overall rate to fall between the two latter cases (Figure 13). These predictions are born out in the computer simulation. Figure 14 shows the effect of increasing the rate of the second reaction from one fifth to ten times the rate of the first.

In addition to the hydrolysis reactions, re-esterification and condensation also involve water, here as a product. Re-esterification is by definition the reverse of the hydrolysis process and has been shown to occur at significant rates for silanes in studies using Karl-Fischer reagent. The result of reversibility being included in the kinetic treatment is to increase gradually the apparent order of the overall reaction as it proceeds.

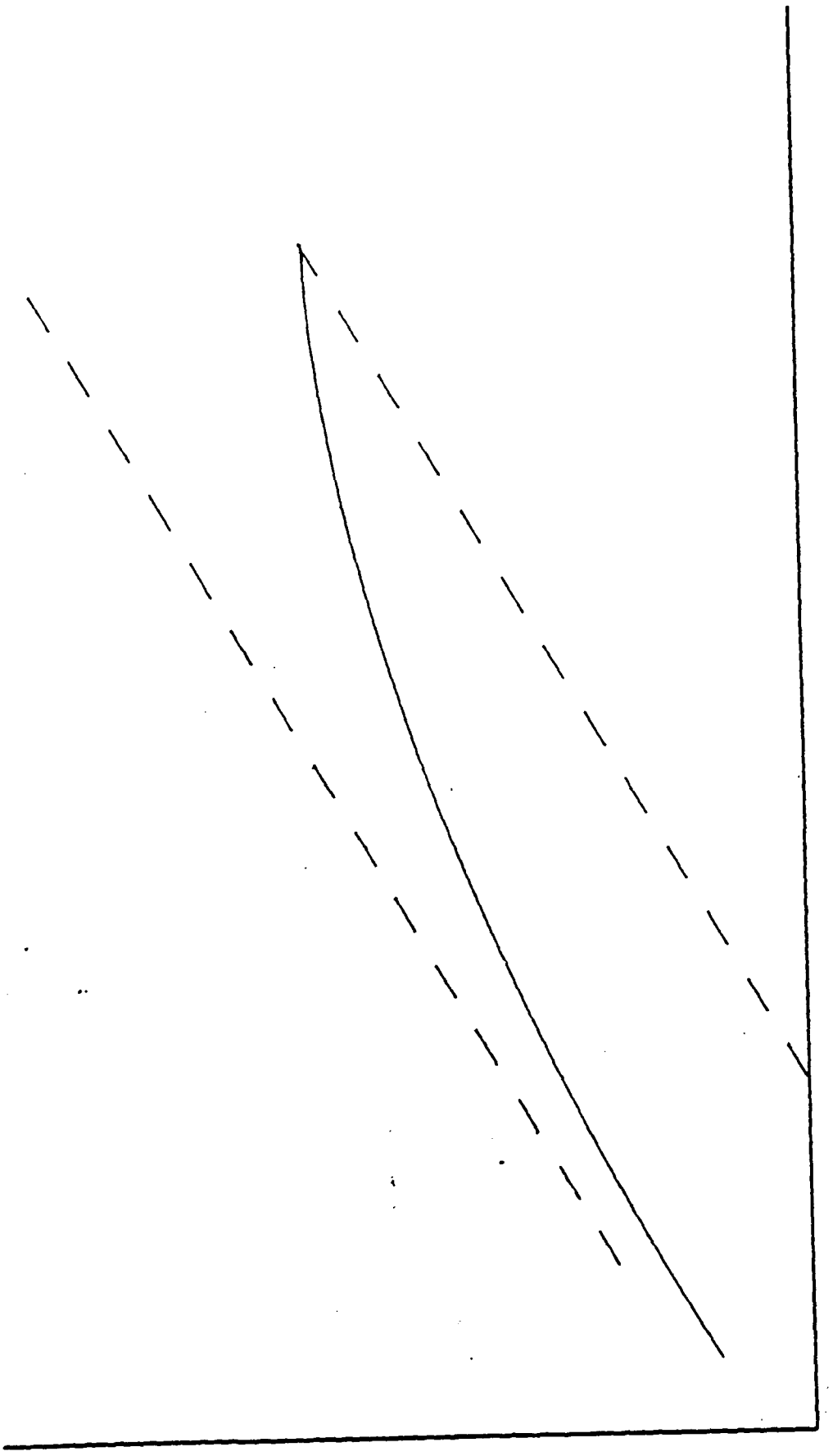

Figure 13

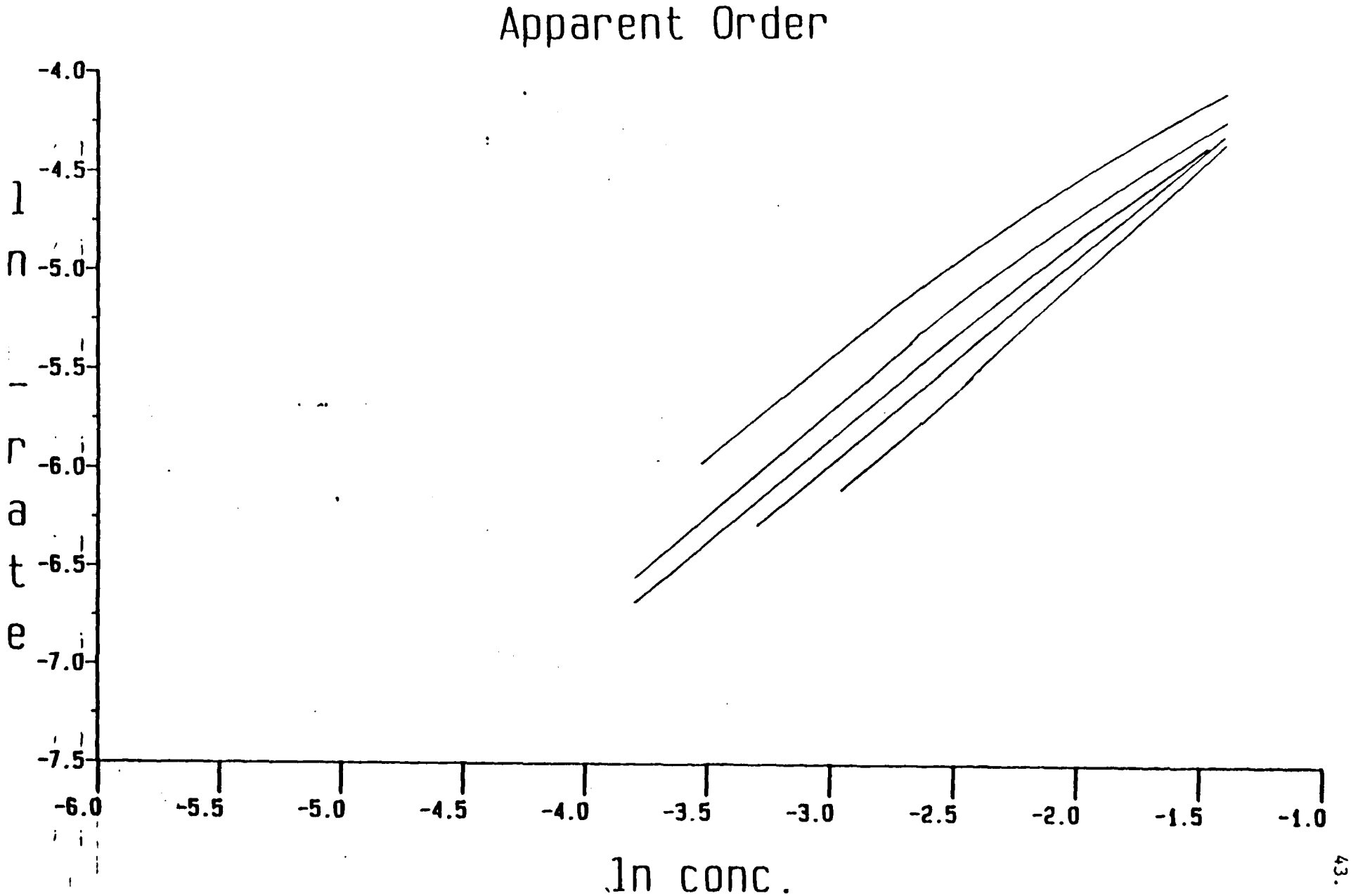
Apparent Order
ln rate
-4.0
-4.5
-5.0
-5.5
-6.0
-6.5
-7.0
-7.5
-6.0
-5.5
-5.0
-4.5
-4.0
-3.5
-3.0
-2.5
-2.0
-1.5
-1.0
ln conc.

Figure 14

Figure 15 shows the result of a computer simulation of re-esterification rates between 0 and 10 percent of the forward rate of one reaction. As seen before, when the hydrolysis reaction is irreversible and the silane species is present in great excess, the resulting apparent order is unity. However, as the rate of the reverse reaction becomes more appreciable, the apparent order increases greatly as the water concentration drops. Finally, as equilibrium is approached the overall reaction rate goes to zero, causing the ln(-rate) vs. ln(conc.) curve to tail off towards negative infinity. As expected, as the rate of the re-esterification process increases, the equilibrium concentration also increases. The usual approach for correcting this effect is to reassign zero as the equilibrium concentration of the monitored species. This serves to make the corrected concentration go to zero at the same rate as the reaction rate, preserving the first order relation.

Condensation is the process by which small species combine to form larger ones. It can be represented by two reactions, one involving water as a product (Equation 15) and the other yielding alcohol (Equation 16).

$$\equiv Si\text{-}OH + HO\text{-}Si\equiv \rightarrow \equiv Si\text{-}O\text{-}Si\equiv + H_2O \qquad (15)$$

$$\equiv Si\text{-}OH + RO\text{-}Si\equiv \rightarrow \equiv Si\text{-}O\text{-}Si\equiv + ROH \qquad (16)$$

Since the latter does not involve water, we will ignore it in this treatment. As before, water produced via reaction (15) cannot be distinguished from water which was the product of re-esterification. However, in this case, the silane product cannot be fed back into the hydrolysis reaction. An extreme example of this would be the hydrolysis and condensation of

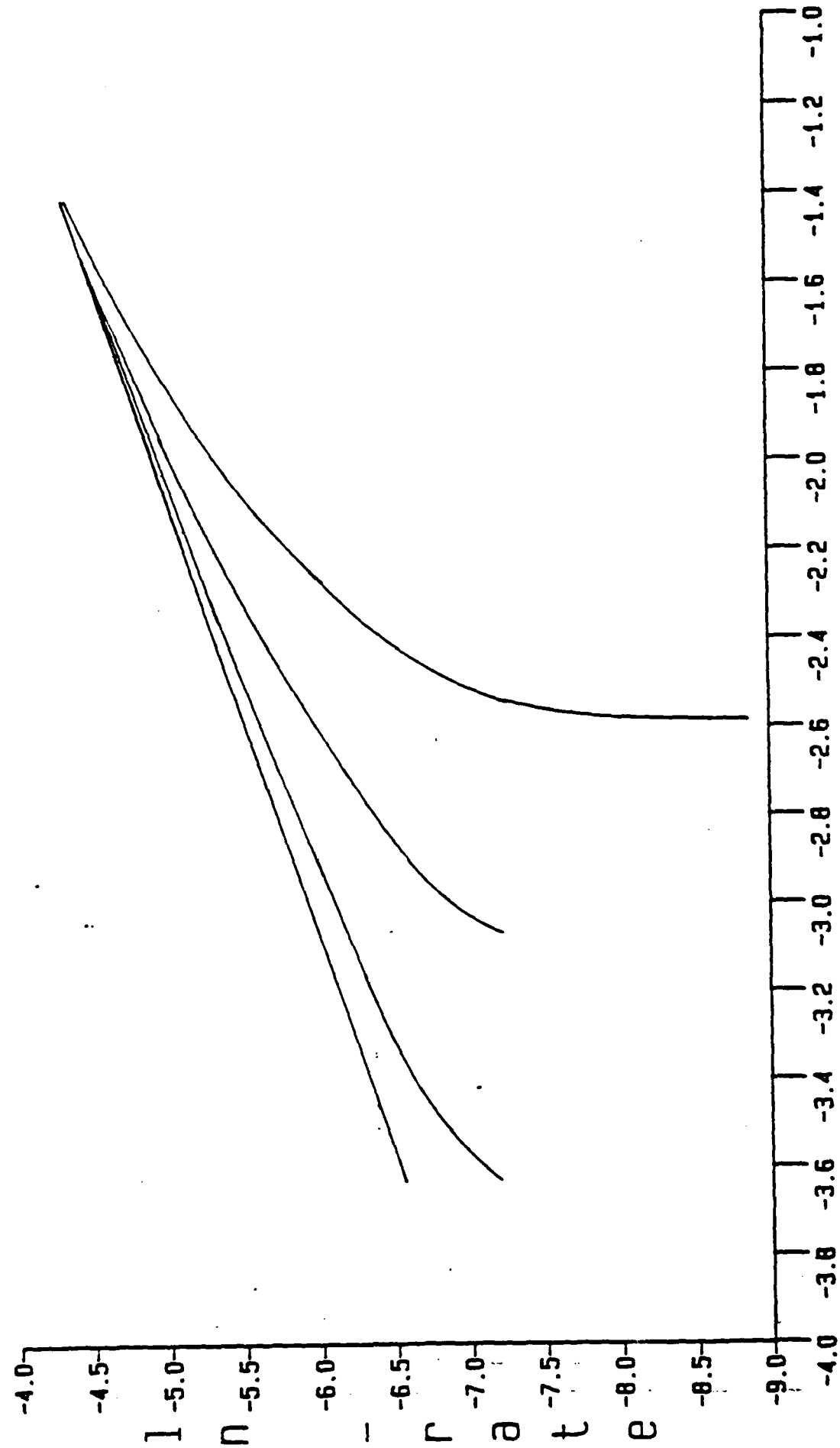
Apparent Order
ln - rate
-4.0
-4.5
-5.0
-5.5
-6.0
-6.5
-7.0
-7.5
-8.0
-8.5
-9.0
-4.0
-3.8
-3.6
-3.4
-3.2
-3.0
-2.8
-2.6
-2.4
-2.2
-2.0
-1.8
-1.6
-1.4
-1.2
-1.0
ln conc.

Figure 15

tetramethylorthosilicate (TMOS) with 4 moles of water per mole of TMOS. Since hydrolysis of TMOS is very fast, all of the reactants would initially combine to form silicic acid, which would then condense. All four moles of water would disappear followed by the reappearance of two. This will cause the rate of disappearance to become negative, and the natural log will become undefined. In TEOS, hydrolysis and condensation occur simultaneously. An added complication is that the condensation rate will be controlled by the mobility of oligomeric species during the later stages of condensation. These processes cannot be modelled with simple kinetics.

The form of the infra-red data obtained in the present work cannot be regarded as surprising in light of the many simultaneous processes occurring. Initial apparent orders less than one can be explained by subsequent steps of the hydrolysis being faster than the first. As the reaction proceeds, re-esterification and condensation become appreciable, and the apparent order will steadily increase. These explanations will account for all of the trends seen.

There are other possible explanations, however. If we assume that the apparent order is in fact unity, a lesser value may be observed for the following reasons: Firstly, the temperature of the fluid inside the IR cell may increase during the reaction due to the exothermic nature of hydrolysis, or heating from the incident infra-red radiation. Secondly, the activity of the hydrogen ions may increase over the course of the reaction as the water concentration decreases and in some cases goes to zero. Thirdly, the partially hydrolysed silane may exert a self-catalytic effect, increasing the rate of the reaction as it proceeds. The first possibility has seemingly been ruled out by workers using a water-cooled temperature-controlled IR cell,

and by ourselves by comparing the reaction rates with varying incident infra-red intensities. We have determined that for our simple non-temperature controlled calcium fluoride cell with a 0.5 mm pathlength (50 times the experimental conditions), a 4°K temperature rise will occur due to beam heating of ethanol. This result must be taken with a grain of salt because the volume to surface ratio has been increased by the same ratio, decreasing the rate at which the heat can be conducted away.

The possibility involving the activity of hydrogen ions also seems unlikely. Our data indicate that the rate of hydrolysis decreases if the concentration of hydrogen ions remains constant but more water is added initially. This is consistent with the pKa of protonated water being higher than that of protonated ethanol; and as the water disappears the hydrogen ions are available to protonate the other solvent species, i.e., ethanol. Based on this, the effect is predicted to be largest in systems where the water just disappears completely. This is contrary to what we observed, where the effect is most acute for the 1:4:4 starting composition.

The third possible explanation, involving an autocatalytic effect of the partially hydrolysed silane has no supporting data, but cannot be ignored as a possibility.

In summary, we have measured the concentration of H_2O as a function of time during the hydrolysis of TEOS using IR spectroscopy. The apparent order of the reaction, as calculated from the water concentration, changed as the reaction proceeded. It is our opinion that this is due in large part to following only one species, water, which is involved in several hydrolysis and condensation reactions. As each of these reactions likely takes place at different rates, the resulting convolution makes the data complex.

In order to overcome this, there are two choices. The first is to measure only the water concentration but to monitor only the start of the reactions for very understoichiometric amounts of water, far below the conditions discussed here and of interest in the development of coatings. Although this may result in a quantitative reaction rate and order, there is some doubt to how applicable these numbers would be to systems with more water. TEOS does not obey simple kinetics, so that there would be much difficulty in extrapolating the data to higher water systems. Alternatively, one could follow the concentration of all species as functions of time. This may be possible with tools such as ^{29}Si NMR if done along the same lines as condensation studies. Although the ensuing analysis would be difficult, it does not seem impossible.

Infra-red spectroscopy does not lend itself well to this task. Absorption bands are generally quite broad and tend to overlap, leading to difficulties in determining how much of any species is actually present. IR techniques do make the determination of water concentration quite easy; and the point at which the free water in solution disappears can be determined without difficulty. Such data are of great utility when partially hydrolysed silanes are added to other faster reacting species. In the past, one has relied upon experience to decide how long after the silane has started hydrolysing to add other species. IR analysis makes this determination quite easy and allows the maximization of M-O-Si bridges.

B. Crystallization vs. Viscous Sintering

Using sol-gel techniques, it is possible to produce fine amorphous powders or dried gels having distributions of fine pores. To obtain dense, glassy bodies or coatings from such materials, it is useful to define regions of time and temperature (or heating rates) where the kinetics of viscous sintering are faster than those of crystallization--assuming that such regions exist for a given material.

In describing viscous sintering, we have used the cylindrical pore model of Scherer. This model is very attractive for bodies of the type produced by sol-gel processes. It employs the basic assumptions of the Frenkel model for the viscous sintering of spheres; and considering these assumptions, it is remarkable that the model predicts experimental data as well as it does (which is quite well).

The model predicts that the time required for appreciable sintering is proportional to the viscosity and inversely proportional to the surface energy. Among microstructural features, the most important feature is the pore radius. The initial particle size and packing density are less significant (particles of difference sizes can be packed differently to give the same pore size, and exhibit similar times for sintering). In the present paper, we have taken pore sizes of 50 Å and 5000 Å to represent the effective limits obtained from sol-gel processing.

The process of crystallization has been described using the approach developed previously in our laboratory. Under isothermal conditions, the times at various temperatures required to reach a just-detectable degree of crystallinity are represented by time-temperature-transformation (TTT) curves; while crystallization under conditions of constant heating rate is

described using the analysis of crystallization statistics. In the present paper, viscous sintering and crystallization are viewed as competitive processes and the analysis of this competition is applied to a number of representative glass-forming liquids.

Considering isothermal conditions, Figure 17 indicates the calculated behavior for a representative organic glass former, o-terphenyl. The regions of time at any temperature between the appropriate sintering curve and the crystallization curve for a just-detectable volume fraction crystallized at 10^{-6} indicate the conditions where densification can be achieved without detectable crystallization. In some cases, the regions of time may be inaccessibly short; but in the case of o-terphenyl, there is a range of conditions under which densification can be obtained without crystallization.

The magnitude of the viscosity at any temperature affects both the sintering rate and the crystallization rate. To take account of the dependence of the viscosity, results such as those shown in Figure 17 may conveniently be plotted as a function of t/η, where η is the viscosity. Such a plot is shown in Figure 18 for anorthite.

For crystallization under conditions of constant heating rate, the competition between crystallization and viscous sintering is conveniently represented in terms of a heating rate vs. temperature relation, such as that shown in Figure 19 for anorthite. As shown there, there exist windows in temperature, over a range of heating rates, in which substantial sintering can take place without the occurrence of detectable crystllization.

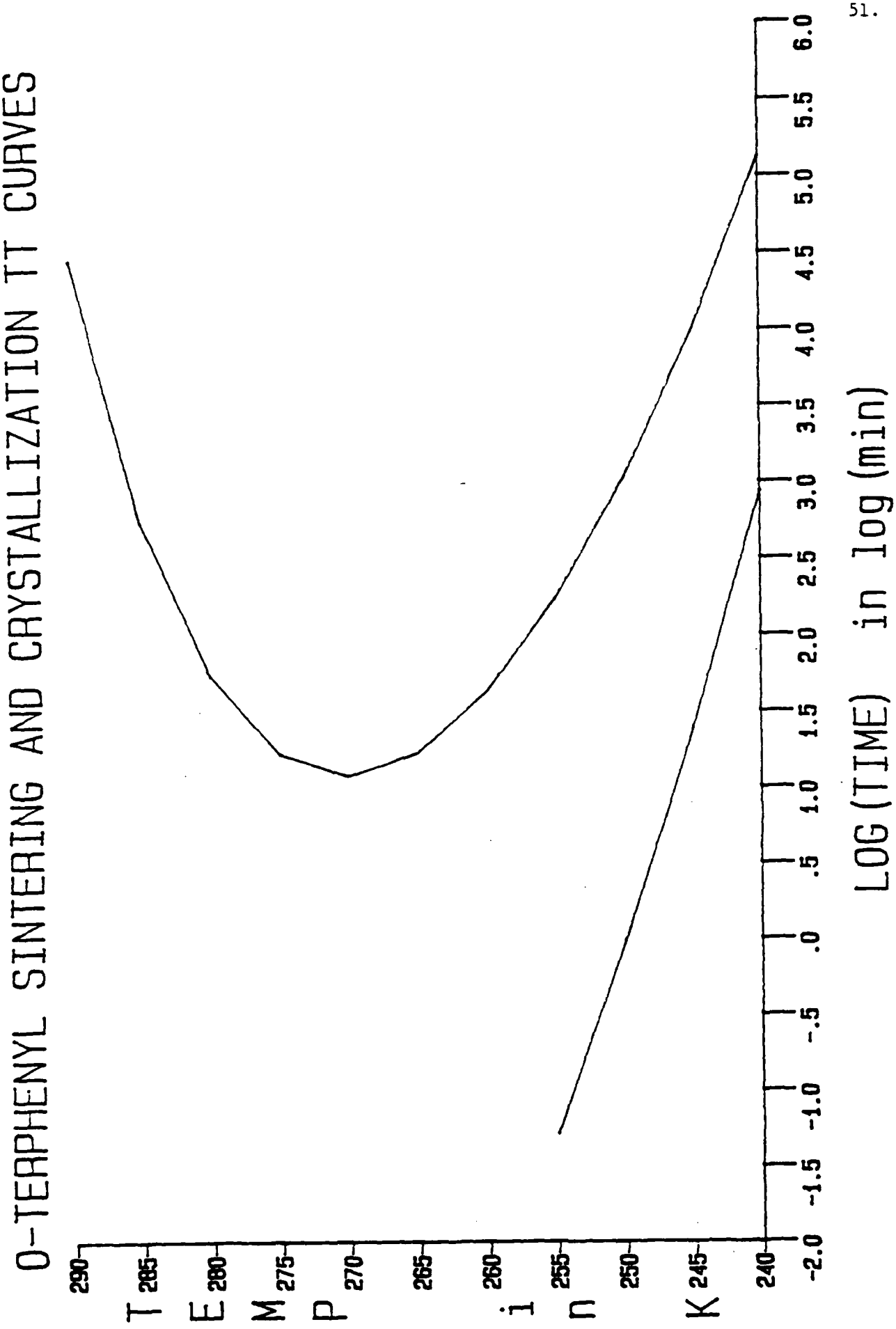
O-TERPHENYL SINTERING AND CRYSTALLIZATION TT CURVES
TEMP in K
290
285
280
275
270
265
260
255
250
245
240
LOG (TIME) in log (min)
-2.0
-1.5
-1.0
-.5
.0
.5
1.0
1.5
2.0
2.5
3.0
3.5
4.0
4.5
5.0
5.5
6.0

Figure 17

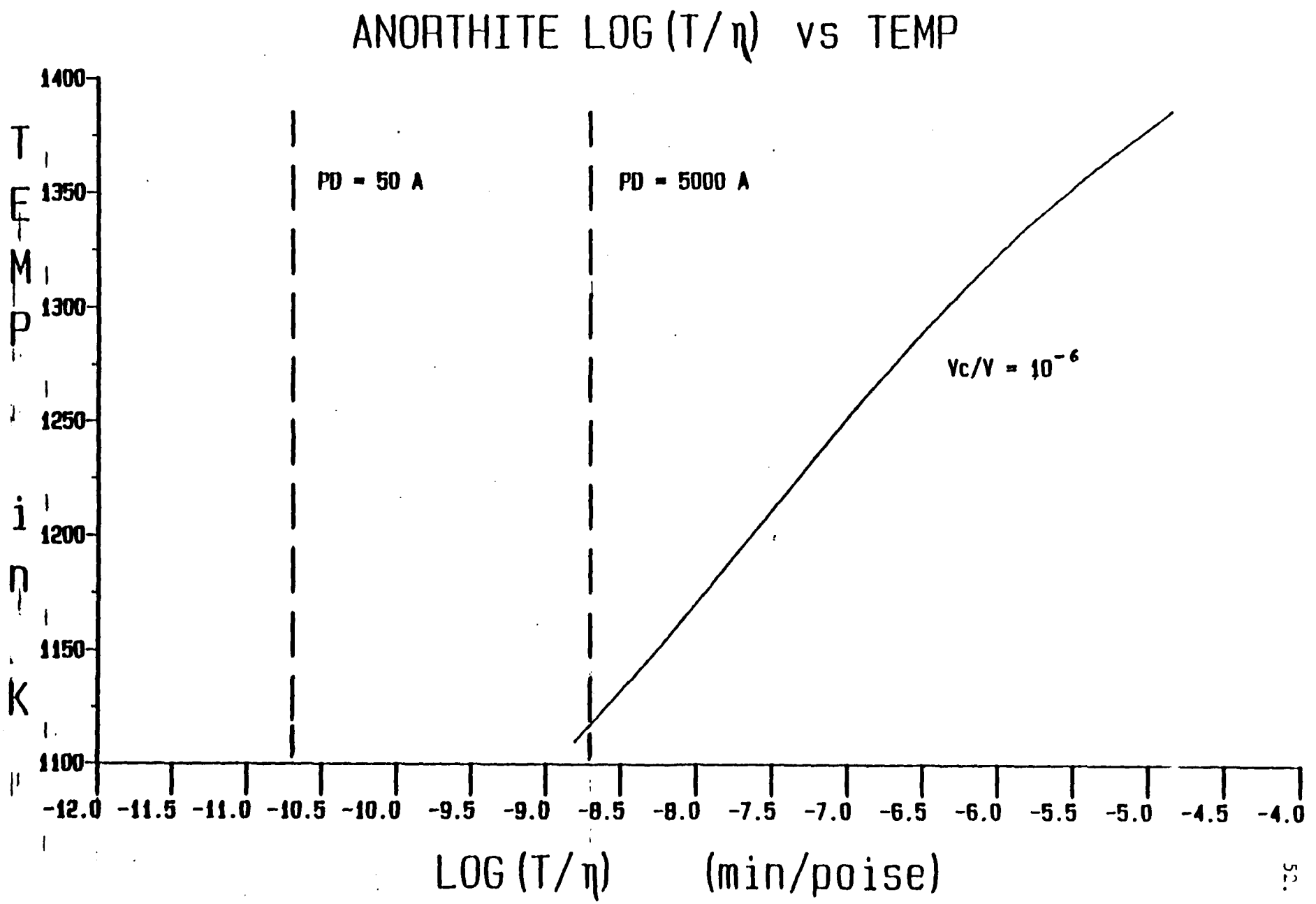
ANORTHITE LOG (T/η) vs TEMP
TEMP in K
1400
1350
1300
1250
1200
1150
1100
PD = 50 A
PD = 5000 A
Vc/V = 10^-6
-12.0 -11.5 -11.0 -10.5 -10.0 -9.5 -9.0 -8.5 -8.0 -7.5 -7.0 -6.5 -6.0 -5.5 -5.0 -4.5 -4.0
LOG (T/η) (min/poise)

Figure 18

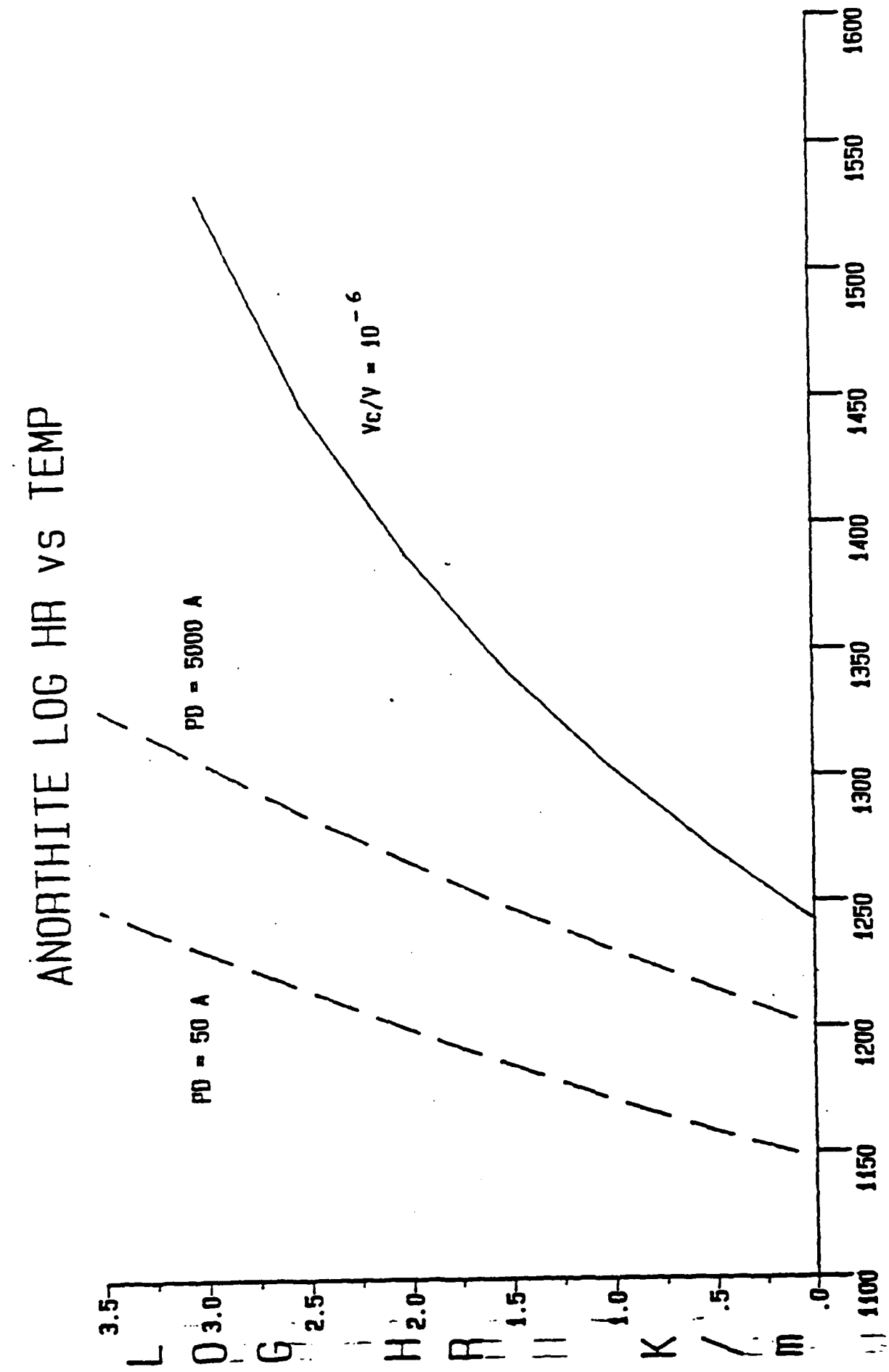
ANORTHITE LOG HR vs TEMP
LOG HR in K/m
3.5
3.0
2.5
2.0
1.5
1.0
.5
.0
1100
1150
1200
1250
1300
1350
1400
1450
1500
1550
1600
TEMPERATURE in K
PD = 50 A
PD = 5000 A
Vc/V = 10^-6

Figure 19

All of the above discussion has used bulk material properties and measured or estimated nucleation barriers, together with the assumption of steady state nucleation rates. The effect of different nucleation barriers on the competition between sintering and crystallization is shown in Figure 20 for anorthite-like materials having various nucleation barriers (represented as BkT). As seen there, with decreasing barrier to crystal nucleation, the processing window in which sintering can be achieved without detectable crystallization is expected to decrease. For sufficiently small nucleation barriers, such as BkT = 40 for a material with the properties of anorthite, crystallization will take place before sintering at all heating rates evaluated. The measured nucleation barrier of anorthite is about 82 kT.

The effect of changes in the degree of crystallinity is shown in Figure 21 for $Na_2O{\cdot}2SiO_2$. Larger processing windows are suggested for conditions where larger volume fractions crystallized are acceptable. Also plotted in Figure 21 are the experimental results of Hench et al., who observed sintering without crystallization in one hour treatments at 753 C - 793 C, and crystallization at temperatures of 793 C - 813 C. Their condition for sintering corresponds to a degree of densification beyond that contemplated in the present calculations, and hence the agreement between predictions and experiment seems quite reasonable.

The assumption of steady state nucleation rates can be relaxed by considering the incubation time during which steady state distributions of subcritical embryos are established. The effect of such transient nucleation is to shift the crystallization curves to higher temperatures and thereby enlarge the processing window. Of the materials considered

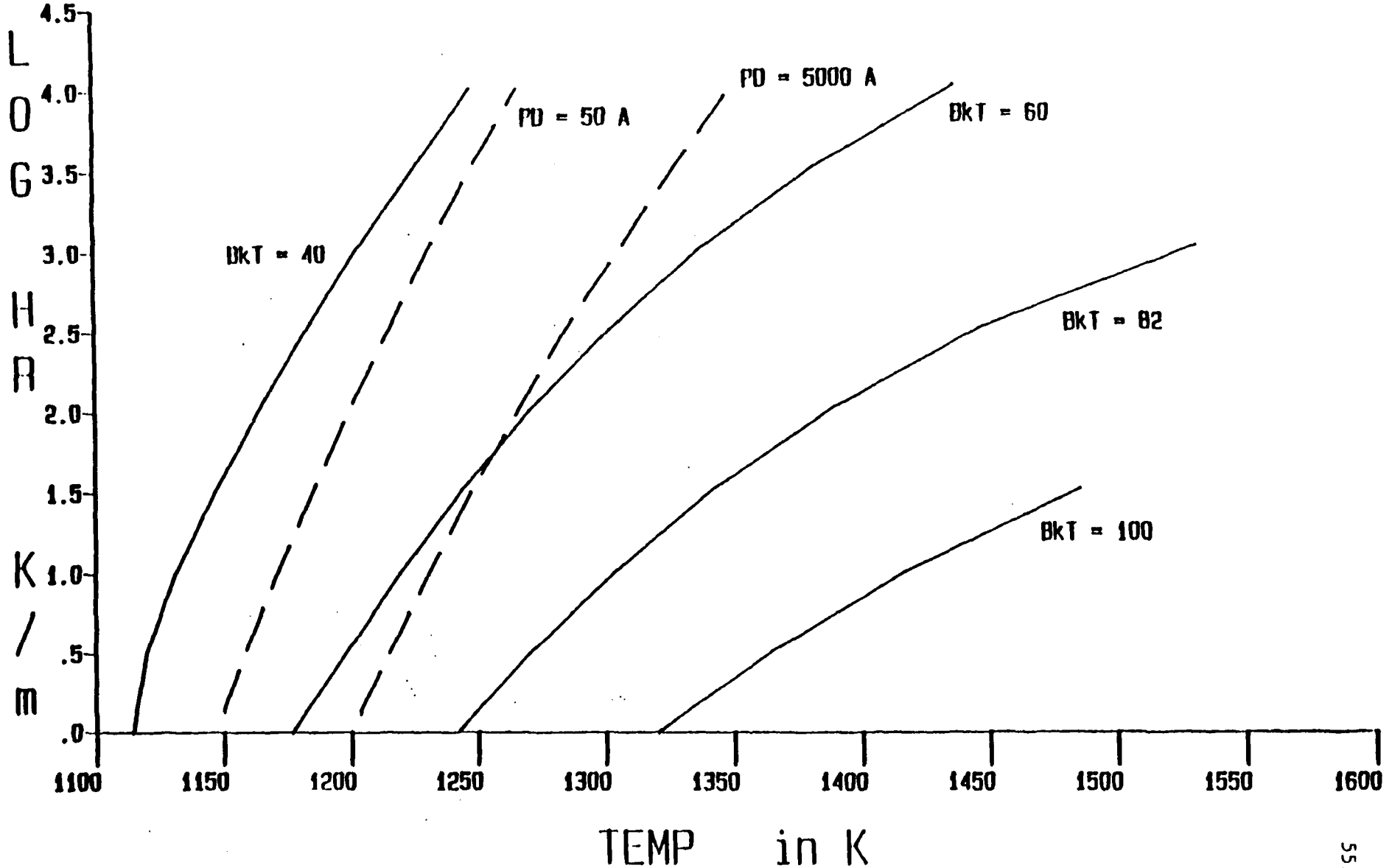
ANORTHITE MATERIALS, VARIABLE BkT, LOG HR vs TEMP
LOG HR Km
4.5
4.0
3.5
3.0
2.5
2.0
1.5
1.0
.5
.0
PD = 5000 A
PD = 50 A
BkT = 60
BkT = 40
BkT = 82
BkT = 100
1100
1150
1200
1250
1300
1350
1400
1450
1500
1550
1600
TEMP in K

Figure 20

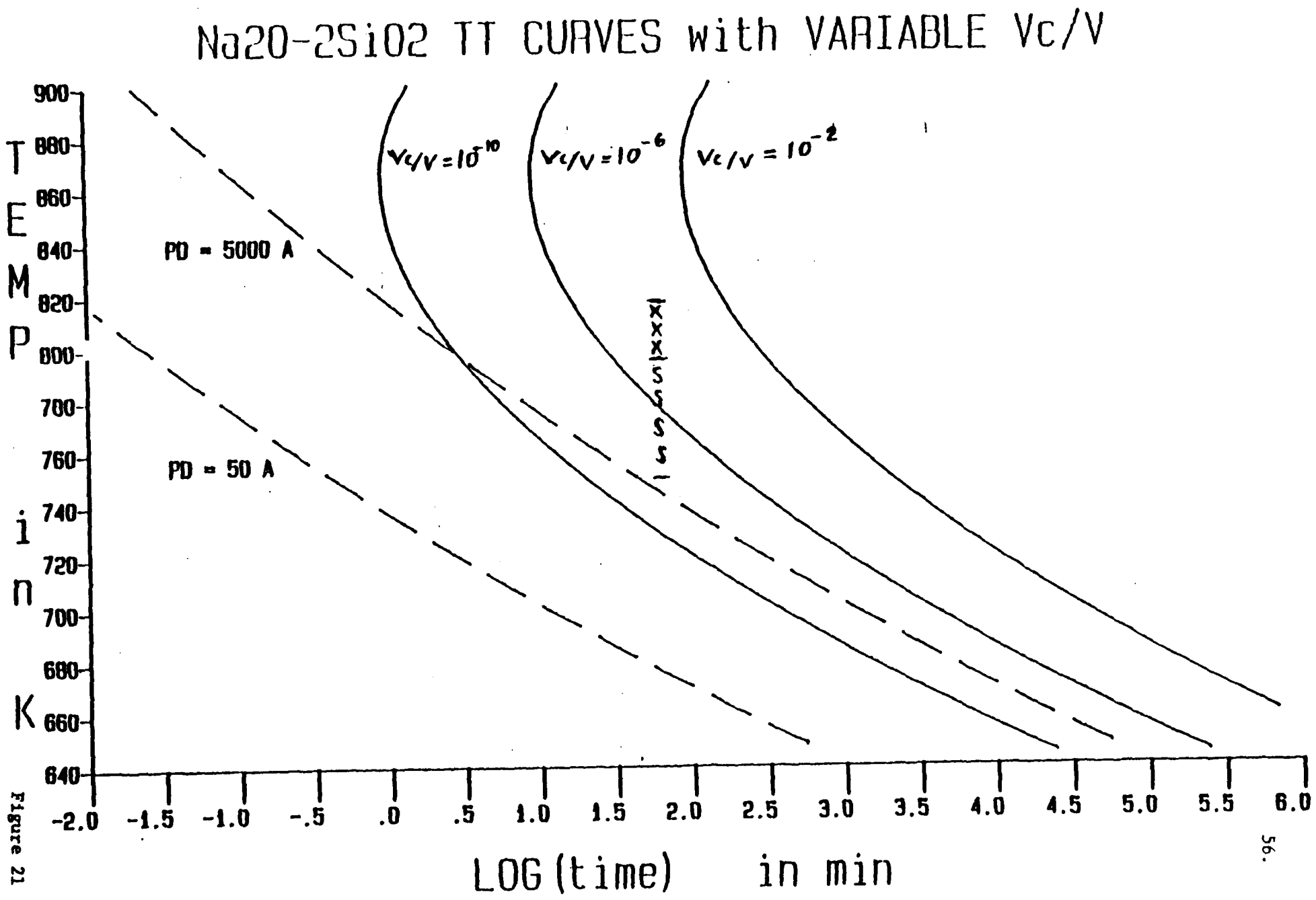
Na2O-2SiO2 TT CURVES with VARIABLE Vc/V
TEMP in K
900
880
860
840
820
800
780
760
740
720
700
680
660
640
PD = 5000 A
PD = 50 A
Vc/V = 10^-10
Vc/V = 10^-6
Vc/V = 10^-2
xxxxxxxxx
-2.0
-1.5
-1.0
-.5
.0
.5
1.0
1.5
2.0
2.5
3.0
3.5
4.0
4.5
5.0
5.5
6.0
LOG (time) in min

Figure 21

in the present study, the effect is most pronounced for $Li_2O \cdot 2SiO_2$, for which the results shown in Figure 22 were obtained.

It is well recognized that sol-gel derived materials are generally characterized by properties, such as liquid viscosities, which differ from those of melted glasses. In applying the present analysis to SiO_2, use has been made of the data of Sacks et al. for the viscosity of the "wet" SiO_2 employed in his studies. The viscosities reported there were appreciably smaller than those of conventional fused silica, and the lower viscosities have an appreciable effect on the expected rates of sintering and crystallization. These are shown in Figure 23. Also shown in the figure are the other results of Sacks, who observed sintering to an amorphous state in 24 hours at 1274 C, but crystallization in 48 hours at 1273 C or 3 hours at 1323 C. The pore size in Sacks' experiments were a few thousand Å. From the results shown in Figure 23, remarkable agreement is seen between the predicted behavior and experimental results.

The effects of other factors on the competition between crystallization and viscous sintering are presently being explored. These include the effects of heterogeneous nucleation as well as the effects of time-dependent properties. Once the results of these calculations are in hand, it should be possible to specify for a given material the conditions of time and temperature in which densification of coatings can be achieved without undesired crystallization (or alternatively, the conditions under which crystallization to desired assemblages of phases can be achieved). This will greatly facilitate the experimental development of coatings for glass having the desired high density (freedom from porosity). It is expected that the theoretical work will be completed by the time that the optimization phase of the respective coating developments is initiated.

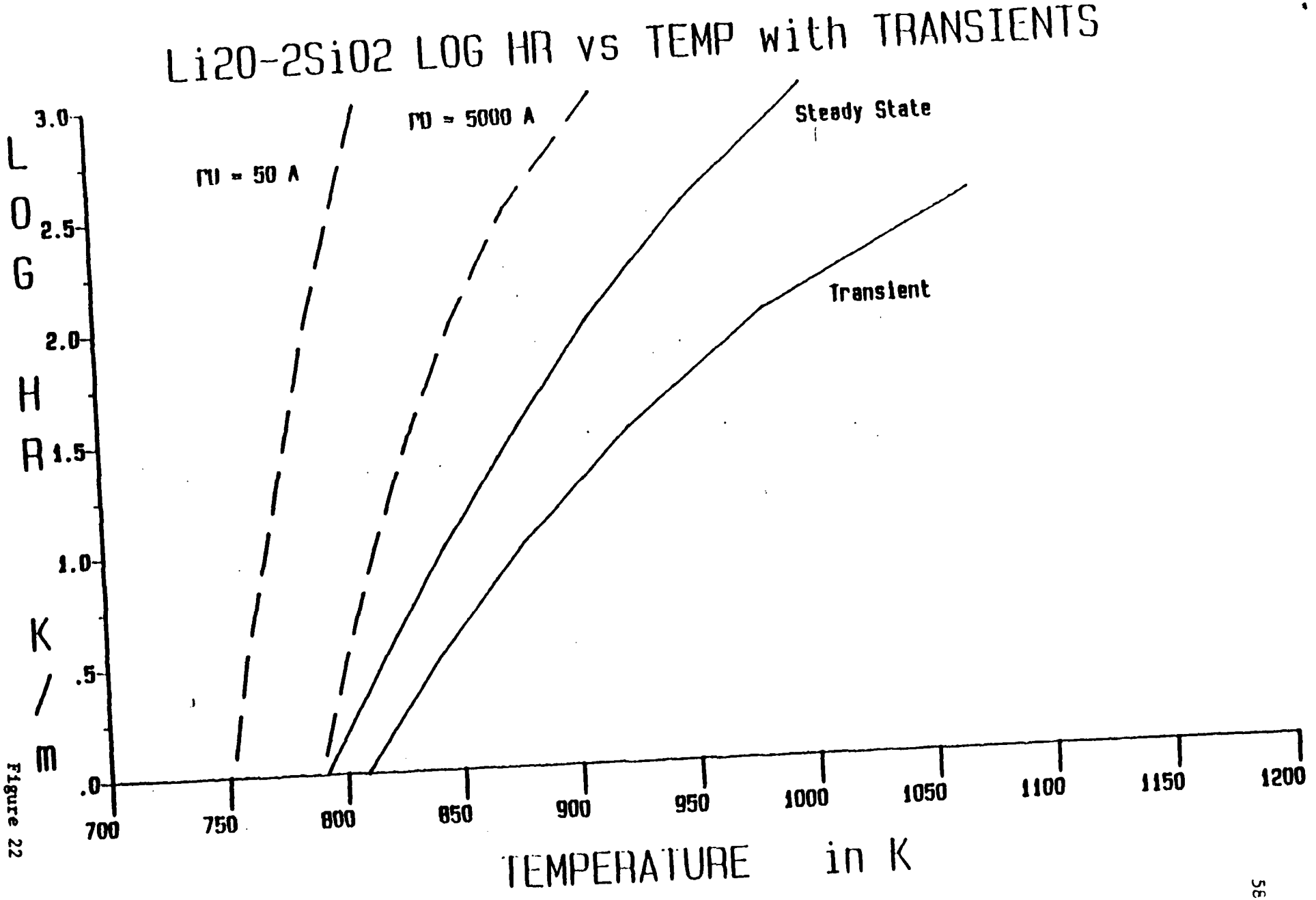
Li2O-2SiO2 LOG HR vs TEMP with TRANSIENTS
LOG HR K/m
3.0
2.5
2.0
1.5
1.0
.5
.0
700
750
800
850
900
950
1000
1050
1100
1150
1200
TEMPERATURE in K
M0 = 50 A
M0 = 5000 A
Steady State
Transient

Figure 22

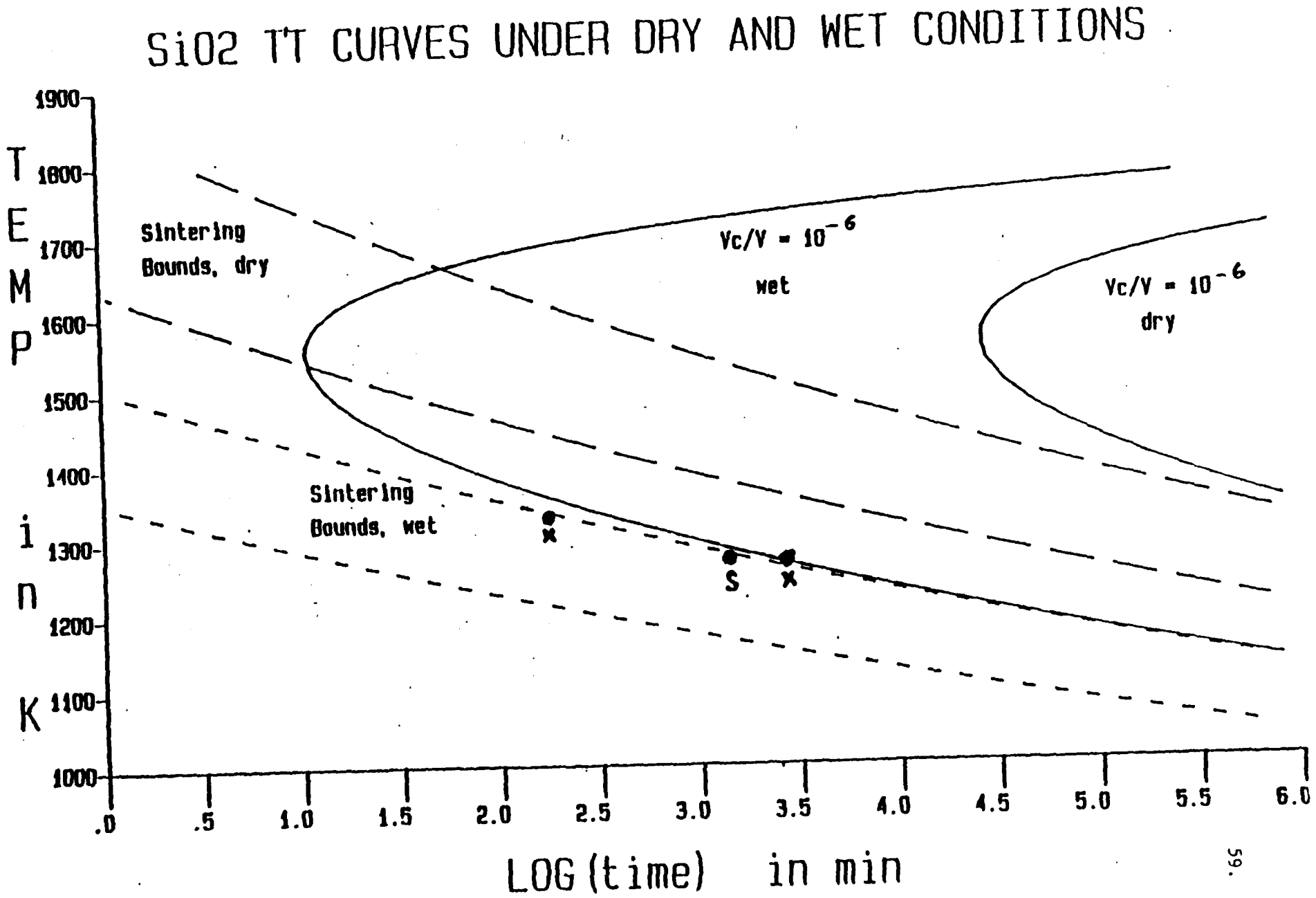
SiO2 TT CURVES UNDER DRY AND WET CONDITIONS
TEMP in K
1900
1800
1700
1600
1500
1400
1300
1200
1100
1000
Sintering Bounds, dry
Sintering Bounds, wet
Vc/V = 10^-6 wet
Vc/V = 10^-6 dry
S
.0
.5
1.0
1.5
2.0
2.5
3.0
3.5
4.0
4.5
5.0
5.5
6.0
LOG (time) in min

Figure 23